

# Constraining a Radiative Transfer Model with Satellite Retrievals: Contrasts between Cirrus Formed via Homogeneous and Heterogeneous Freezing and their Implications for Cirrus Cloud

## 5 Thinning

Ehsan Erfani<sup>1</sup> and David L. Mitchell<sup>1</sup>

<sup>1</sup>Division of Atmospheric Sciences, Desert Research Institute, Reno, Nevada, USA

Correspondence to: Ehsan Erfani, ([Ehsan.Erfani@dri.edu](mailto:Ehsan.Erfani@dri.edu))

10

### Abstract

The complex mechanisms governing the formation of cirrus clouds pose significant challenges in the accurate simulation of cirrus clouds within climate models, leading to uncertainties in predicting the cirrus cloud response to aerosols and efficacy of cirrus cloud  
15 thinning (CCT), a *climate intervention* method. One issue is related to the relative contributions of homogeneous and heterogeneous ice nucleation. Recent satellite observations from the Cloud-Aerosol Lidar and Infrared Pathfinder Satellite Observation (CALIPSO) suggest that cirrus clouds strongly affected by homogeneous ice nucleation (i.e., homogeneous cirrus) play a more important role than previously assumed. We employ a radiative transfer model to quantify the cloud radiative  
20 effect for homogeneous and heterogeneous cirrus clouds at the top of atmosphere (TOA), Earth's surface, and within the atmosphere. The experiments are conducted using cirrus ice water content and effective diameter vertical profiles from CALIPSO retrievals for homogeneous and heterogeneous cirrus clouds across different regions (Arctic, Antarctic, and midlatitude) and surface types (ocean and land). Results indicate that homogeneous cirrus clouds exhibit stronger  
25 radiative effects than heterogeneous cirrus, implying that transitioning from homogeneous to heterogeneous cirrus, as an indicator of CCT efficacy, could induce substantial surface cooling, particularly in polar regions during winter. However, “new cirrus” formation decreases that effect,

leading to an estimated instantaneous surface cooling effects range from -0.2 to -0.5 W m<sup>-2</sup>, with the TOA cooling reaching up to -0.9 W m<sup>-2</sup>. This study highlights the need for improved  
30 representation of homogeneous cirrus in models to better predict the cirrus cloud climatic impacts and the CCT viability.

## 1 Introduction

Cirrus clouds are a critical component of the Earth's radiation budget; the global annual mean coverage of these clouds ranges from 17-20% (Matus and L'Ecuyer, 2017; Sassen et al., 2009) to  
35% (Hong et al., 2016) with high spatial variability. Cirrus cloud coverage is about 30% in mid-latitudes and about 60-80% in the tropics (Guignard et al., 2012; Stubenrauch et al., 2006). In addition, cirrus clouds are more frequent during the winter seasons in the mid and high latitudes (Mitchell et al., 2018; Zhu et al., 2024). They significantly absorb and scatter incoming solar radiation and absorb outgoing thermal radiation from the Earth's surface and low-level clouds.  
40 Although these two effect counteract each other, it is estimated that on global annual averages, these clouds warm the planet by approximately 5 W m<sup>-2</sup> (Gasparini and Lohmann, 2016). Despite their significant impacts on radiation and climate, uncertainty exists in measuring, retrieving, and modeling cirrus clouds partly because the processes involved in their formation are poorly understood (Heymsfield et al., 2017) or are not represented in climate models (Lyu and Liu, 2023).  
45 This complexity has left many important questions unanswered (Kärcher, 2017; Kay et al., 2012). In particular, our understanding of the mechanisms of cirrus cloud development and their microphysical properties, such as ice crystal shape and size distribution remain insufficient (Krämer et al., 2016; Lawson et al., 2019). Cirrus clouds exhibit diverse geometric features (Fig. 1), which reflect their varied microphysical and macrophysical properties.  
50 One of the main uncertainties in modeling cirrus clouds is related to insufficient knowledge of the relative contribution of homogeneous and heterogeneous ice nucleations in cirrus clouds (Heymsfield et al., 2017). Homogeneous ice nucleation happens when liquid solution droplets (haze or cloud droplets) freeze spontaneously, with no ice nucleating particles (INPs) to initiate freezing. This is when the temperature ( $T$ ) is colder than -38 °C and supersaturation (quantified by  
55 relative humidity with respect to ice or RH<sub>i</sub>) is greater than 140-150%. In contrast, heterogeneous ice nucleation requires INPs to initiate freezing at warmer  $T$  and lower RH<sub>i</sub> values (Heymsfield et

al., 2017; Kanji et al., 2017). Since INP concentrations are generally much lower than solution droplet concentrations, heterogeneous cirrus usually have fewer and larger ice particles, and therefore are optically thinner, whereas homogeneous cirrus generally contain higher ice particle 60 concentrations of smaller size, and are optically thicker (Krämer et al., 2016). With such distinct microphysical properties, these two types of cirrus clouds demonstrate significantly different radiative effects, and this makes it crucial to investigate their contributions.

There are different methods to retrieve cirrus cloud properties using satellite instruments such as infrared radiometers (Magurno et al., 2020; Mitchell et al., 2018; Nazaryan et al., 2008; 65 Stubenrauch et al., 2008; Yue et al., 2020), visible radiometers (Gao et al., 2002; Wang et al., 2019), microwave radiometers (Evans et al., 2012; Jiang et al., 2019; Wu et al., 2014), and a combination of instruments (Yorks et al., 2023). Satellite microwave radiometers have been used widely to retrieve cirrus clouds, however, their coarse spatial (Wang et al., 2001) and temporal (Jiang et al., 2019) resolutions, the sensitivity of the retrievals to surface reflectivity (Wang et al., 70 2001), and the need for ancillary information from the surface to properly estimate the surface albedo (Jiang et al., 2019) limit their ability for studying the cirrus clouds. Visible retrievals also have limitations such as low sensitivity to detecting cirrus clouds (especially, thin ones since they have low reflectivity and absorption in the visible range) and contamination of land surface



75 Figure 1. Left: Photography of sky over Reno, Nevada, USA on 25 Sep. 2023, showing cirrus clouds with various geometric features (e.g., thin and thick) (Photo taken by Ehsan Erfani). Right: Satellite imagery showing the same types of cirrus on the same day. Reno is located between Lake Tahoe and Pyramid Lake and is covered by clouds. 80 Note that the two photos do not correspond to the same time, but provide general cloud patterns on the same day (the satellite image provided by MODIS instrument onboard NASA Terra satellite and taken from NASA Worldview website: <https://worldview.earthdata.nasa.gov/>).

reflectance (Schläpfer et al., 2020). On the other hand, infrared retrievals have a much lower  
85 sensitivity to surface reflectivity and can detect thin cirrus clouds using water vapor absorption  
bands (Roskovensky and Liou, 2003).

The Cloud-Aerosol Lidar and Infrared Pathfinder Satellite Observations (CALIPSO) dataset has  
been used to study cirrus cloud properties (Li and Groß, 2021; Sassen et al., 2009). It also has  
90 some limitations; for instance, lidar-radar (DARDAR) retrievals of the ice particle number  
concentration ( $N_i$ ) are based on assumptions about the shape of the ice particle size distribution,  
which can lead to uncertainties in the retrieved values (Sourdeval et al., 2018). Despite this, the  
CALIPSO dataset remains a valuable tool for studying cirrus clouds and their radiative impacts on  
climate. Recently, Mitchell and Garnier (2024) expanded on Mitchell et al. (2024) work and  
developed a CALIPSO retrieval to quantify homogeneous and heterogeneous cirrus on a global  
95 scale (note that the accurate terms would be “dominated by homogeneous” and “dominated by  
heterogeneous” ice nucleation regimes, but for simplicity, we use the terms homogeneous and  
heterogeneous in this study). The data from two Infrared Imaging Radiometer (IIR) channels, 10.6  
μm and 12 μm, were used to calculate ice optical and microphysical properties, such as  $N_i$ , IWC,  
 $D_e$ , and shortwave extinction coefficient ( $\alpha_{ext}$ ) using ice particle mass-dimension and area-  
100 dimension relationships from Erfani and Mitchell (2016). To establish a threshold transition  
between homogeneous and heterogeneous cirrus regimes (henceforth, referred to as cirrus  
regimes), they considered the  $D_e$  maximum in the  $\alpha_{ext}$  -  $D_e$  plane as this threshold (note that high  
 $N_i$  should limit ice particle growth and  $D_e$  due to increased competition for water vapor). In  
particular, they showed that although heterogeneous cirrus is dominant in most regions and  
105 seasons, the homogeneous fraction weighted by cloud optical depth contributes more than 50%  
during the winter in the extratropics.

The findings by Mitchell and Garnier (2024) have important implications for a *climate intervention*  
technique called *cirrus cloud thinning* (CCT). Climate change has disastrous effects on humans,  
the environment, and society, and such effects exacerbate as global CO<sub>2</sub> level and sea surface  
110 temperature (SST) increase (IPCC report, 2021). The last time with CO<sub>2</sub> concentration near 400  
ppm was during the mid-Pliocene (3.25 million years ago) when global SST was 4.1°C warmer  
than preindustrial period (Tierney et al., 2025). Global climate models (GCMs) project that global  
warming will continue in the next decades (IPCC report, 2021), and even in the unlikely scenario

where global greenhouse gas (GHG) emissions are eliminated by 2050 (Forster et al., 2021; 115 Hansen et al., 2023; 2025), the global mean temperature would remain around its 2050 value for centuries unless atmospheric GHG concentrations were decreased somehow. This has prompted some to advocate for a threefold solution: (1) GHG emission reductions, (2) GHG concentration reduction, and (3) climate interventions to cool the planet (Baiman et al., 2024). Solution (3) would take only several years to act, whereas solutions (1) and (2) would take several decades and thus 120 risk triggering tipping points in the climate system (e.g., Steffen et al., 2018). Therefore, various climate intervention methods, including CCT (e.g., Gasparini and Lohmann, 2016; Mitchell and Finnegan, 2009), have been proposed to cool the planet (NASEM report, 2021). It is important to conduct comprehensive research on climate intervention methods in order to quantify their 125 efficacy, cost, risks, and limitations. Climate intervention methods, if proven effective, are not replacements for but rather complement GHG emission reduction and removal.

CCT is a proposed climate intervention method often considered under the Solar Radiation Modification (SRM) category and is suggested to deliberately slow down the warming of the planet by injecting proper aerosols that act as ice nuclei particles (INPs) in the upper troposphere to reduce the thickness and coverage of cirrus clouds (Mitchell and Finnegan, 2009). CCT can be 130 efficient and cool the planet if the homogeneous cirrus is abundant, leading to a “transition from homogeneous to heterogeneous cirrus” (Note: throughout this study, this phrase refers to the concept that the presence of INPs, either through deliberate injection for CCT purposes or through natural and anthropogenic aerosols, can shift the ice nucleation pathway from homogeneous toward heterogeneous, potentially modifying cirrus radiative effects). Heterogeneous cirrus is 135 considered to be dominant outside of tropics (Cziczo et al., 2013; Froyd et al., 2022), but recent satellite retrievals (Gryspeerdt et al., 2018; Mitchell et al., 2018; Mitchell and Garnier, 2024) have shown that homogeneous cirrus might have been underestimated. The effectiveness of CCT might surpass previous estimates, considering that the cooling efficacy of CCT depends on the fraction of homogeneous cirrus. CCT is most impactful in the mid- and high-latitudes during the colder 140 months because the cirrus longwave (LW) cloud radiative effect (CRE) is significantly stronger than shortwave (SW) CRE, and therefore significant surface cooling could happen. Efficient CCT has the potential to reduce the thawing of Arctic permafrost and to enhance the sea ice cover (Storelvmo et al., 2014), and thus enhance the Atlantic Meridional Overturning Current (AMOC)

145 by cooling sea surface temperatures to promote downwelling just south of Greenland. Note that the AMOC is a climate tipping point (Steffen et al., 2018). Moreover, CCT could slow down Arctic amplification (AA), a phenomenon characterized by warming of the Arctic at a rate two to four times faster than the rest of the globe mainly because of sea ice loss (Rantanen et al., 2022; Screen and Simmonds, 2010).

150 Despite the cooling potential of CCT from theory (e.g., Lohmann and Gasparini, 2017; Mitchell and Finnegan, 2009), the results of modeling studies on CCT are not conclusive as some CCT simulations indicated that CCT cooling is negligible (Gasparini & Lohmann, 2016; Penner et al., 2015; Tully et al., 2022) while others (Gruber et al., 2019; Storelvmo et al., 2013, 2014) showed that such cooling is significant. GCMs and regional climate models (RCMs) have significant 155 uncertainties in predicting the microphysical properties of cirrus clouds largely because of limitations in capturing the complicated set of under-resolved physical mechanisms associated with cirrus clouds and their interactions with aerosols (Eliasson et al., 2011; Kay et al., 2012; Maciel et al., 2023; Patnaude et al., 2021). Some possible ways for improving the treatment of CCT in GCMs are described in Mitchell and Garnier (2024) and in Sect. 5 of this study. For this reason, it is important to constrain models with observations to achieve a better understanding of 160 cirrus clouds in general and CCT in particular.

165 An additional concern in the context of CCT is the risk of “overseeding,” where excessive injections of INPs could lead to too many small ice crystals, increasing the optical thickness and the lifetime of cirrus clouds, and thus causing a net warming effect instead of cooling (Gasparini and Lohmann, 2016; Penner et al., 2015). Another potential aspect of overseeding is the formation of “new cirrus” due to INPs injected into clear-sky ice-supersaturated regions (Tan et al., 2016). Observational evidence indicates that stratospheric plumes of enriched INP concentration from 170 volcanic eruptions, upon entering the troposphere, can increase cirrus cloud cover by about 20% (Lin et al., 2025; Sporre et al., 2022), suggesting that CCT seeding may have a similar impact. The extent to which this “new cirrus” effect might offset or even dominate the intended homogeneous-to-heterogeneous transition remains unknown. However, in this study, we address this potential counteracting mechanism.

To evaluate CCT's cooling potential without the use of climate models, a radiative transfer model (RTM) is employed in this study. Over the past decades, RTMs have been used extensively to study the radiative properties of cirrus, contrail, and mixed-phase clouds, since RTMs are the most accurate tools for calculating radiative fluxes when ice cloud microphysical fields are measured (which is difficult to reproduce in a complex GCM). RTMs have been used to determine heating rates and/or the radiative effect of ice clouds, with their microphysical characteristics sometimes measured during aircraft field campaigns (Marsing et al., 2023), retrieved from satellite measurements (Hong et al., 2016; Sun et al., 2011), or simulated by models such as box-models (Cirisan et al., 2013) or models used as stochastic cloud generators (Fauchez et al., 2017; Zhou et al., 2017) or a mesoscale cloud model complex (Khvorostyanov and Sassen, 1998). RTM simulations of cirrus clouds show that their radiative effects are highly sensitive to cloud microphysical characteristics such as ice water path (Córdoba-Jabonero et al., 2020; Fu and Liou, 1993), and ice particle shape and size (Macke et al., 1998; Takano et al., 1992; Zhang et al., 1999). A few studies (e.g., Schumann et al., 2012; Wolf et al., 2023) considered multiple microphysical and environmental parameters (e.g., temperature, surface albedo, solar zenith angle) when computing the radiative effect of cirrus and contrails. Despite significant progress in calculating cirrus cloud radiative properties by using an RTM, the contribution of homogeneous and heterogeneous cirrus to the total cirrus CRE and the efficacy of CCT has not been studied yet.

This study aims to combine new advances in satellite remote sensing and radiative transfer modeling to develop a conceptual platform for studying different types of cirrus clouds and their impact on Earth's energy budget. We use the novel CALIPSO satellite retrievals from Mitchell et al. (2024) to infer the microphysical properties of cirrus clouds (e.g., IWC and  $D_e$ ) and then employ those as inputs to an RTM to calculate cirrus CREs. This is done by calculating the vertical profiles of IWC and  $D_e$  for two types of cirrus clouds (homogeneous and heterogeneous) and different environmental conditions (latitude bands, surface types, seasons) based on CALIPSO retrievals. These are then used in an RTM to calculate cirrus cloud CRE at the surface (Sfc), at top of the atmosphere (TOA), and in the column of atmosphere (Atm). By investigating the difference in CRE between homogeneous and heterogeneous cirrus, this study provides an estimate of the efficacy of CCT as a first estimate, with implications for improving GCMs. This study is specifically focused on the Arctic and Antarctic during the cold season because these are

conditions which (i) homogeneous cirrus occurrence is highest, and (ii) the CCT intervention is expected to have the largest radiative impact due to zero or very weak solar radiation. This targeted design within an RTM framework was intended to support a process-level understanding of cirrus 205 radiative effects and the implications for CCT. The rest of this paper is organized as follows: in Section 2, a description of the observational data and RTM experimental design is presented; the main RTM results are explained in Section 3 for relevant geographical conditions; the sensitivity to thermodynamic profiles, low clouds, and aerosols are explored in Section 4; suggestions for improving cirrus cloud modeling of CCT is provided in Section 5; and finally, conclusions are 210 presented in Section 6.

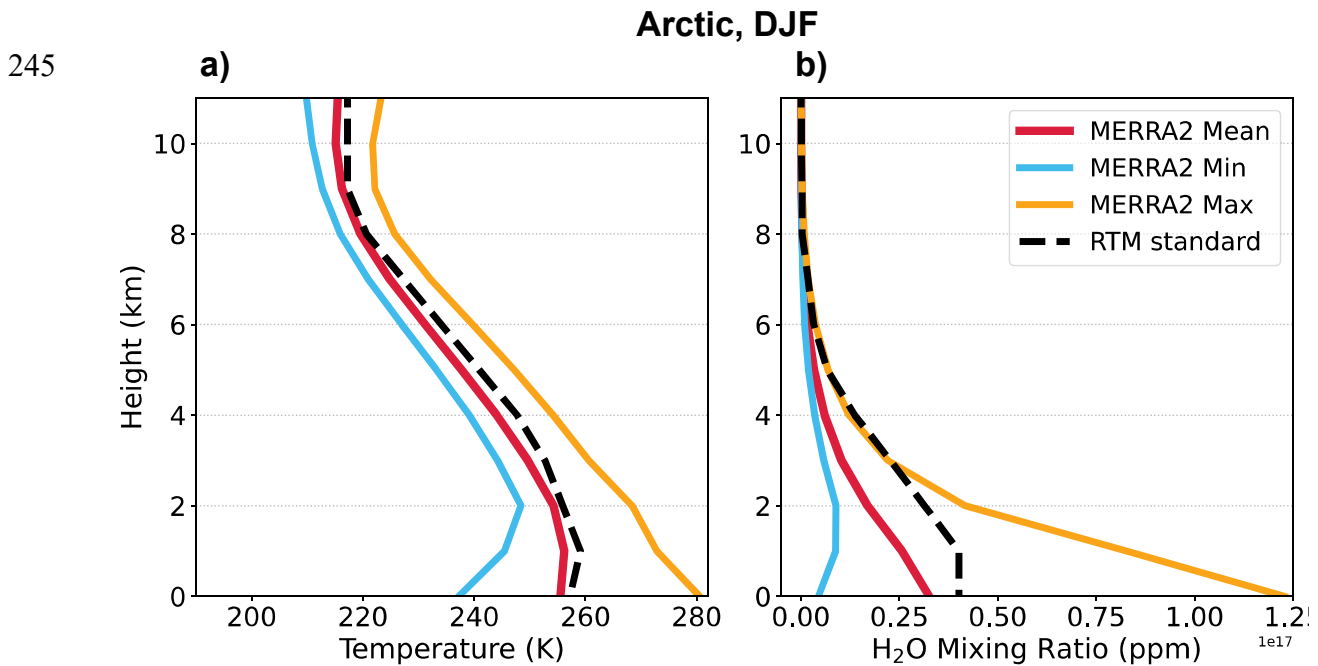
## 2 Methodology

### 2.1 Data

The RTM requires the vertical profiles of atmospheric variables and trace gases as inputs and by 215 default, uses available standard profiles for the tropics, mid-latitude, sub-arctic, and U.S. regions for winter and summer seasons and from surface to 120 km provided by Air Force Geophysical Laboratory (AFGL) atmospheric constituent dataset (Anderson et al., 1986). The radiative impacts of trace gases are small, so we use the standard vertical profiles of trace gases. However, the cirrus cloud properties are closely related to thermodynamic profiles, in particular temperature ( $T$ ). 220 Therefore, to force the RTM with realistic thermodynamic profiles, we replace the standard vertical profiles of  $T$  and water vapor mixing ratio ( $q_v$ ) with those extracted from Modern-Era Retrospective Analysis for Research and Applications, version two (MERRA2; Gelaro et al., 2017) reanalysis dataset with a spatial resolution of  $0.5 \times 0.625^\circ$ , 72 vertical levels, and a temporal resolution of 1 month. Using this dataset is preferred because it was also used in the CALIPSO 225 satellite retrievals of homogeneous and heterogeneous cirrus clouds. The RTM requires air density ( $\rho_a$ ) to be consistent with thermodynamic profiles, therefore, we calculate  $\rho_a$  based on MERRA2  $T$  and pressure ( $P$ ) following the ideal gas law:  $\rho_a = P/kT$ , where  $k$  is Boltzmann constant. This new  $\rho_a$  then replaces the default  $\rho_a$ . The area-weighted averages of  $T$ ,  $q_v$ , and  $\rho_a$  profiles are calculated for grid points in the Arctic (60-90°N), Antarctic (90-60°S), and the Northern Hemisphere (NH)

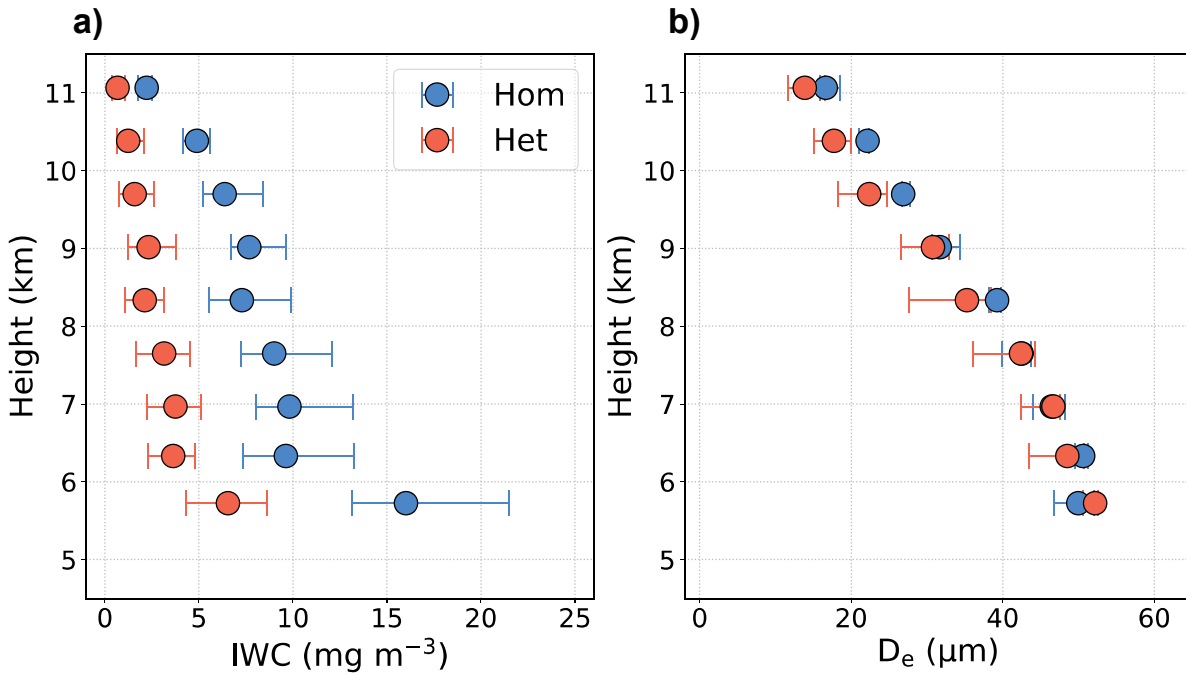
230 mid-latitude (30-60°N), and for winter seasons of the same years as the CALIPSO retrievals (2008, 2010, 2012, and 2013). In addition, maximum and minimum profiles in each region are calculated as a range of change in thermodynamic variables (Fig. 2). Using RTM standard sub-arctic profiles are not justified, because they over-estimate the cold and dry profiles over the Arctic.

235 The CALIPSO satellite retrievals based on the methodology of Mitchell et al. (2024) and Mitchell and Garnier (2024) are used to create cirrus cloud property statistics (e.g., median and 25<sup>th</sup> and 75<sup>th</sup> percentiles) for each season, latitude band, and surface type (land or ocean). In addition, the data is grouped into homogeneous and heterogeneous cirrus categories, based on temperature-dependent  $\alpha_{ext}$  thresholds derived from  $D_e$  maxima (related to the  $\alpha_{ext}$ ) as established by those studies. The reader is advised to check Mitchell and Garnier (2024) for a detailed explanation of 240 the method for discriminating between heterogeneous and homogeneous cirrus clouds, but we can say that the microphysical properties of the latter are strongly affected by homogeneous nucleation. Figure 3 shows an example of this analysis for IWC and  $D_e$  vs. height over the Arctic during the December-January-February (DJF) period. Note that each panel presents a compilation of



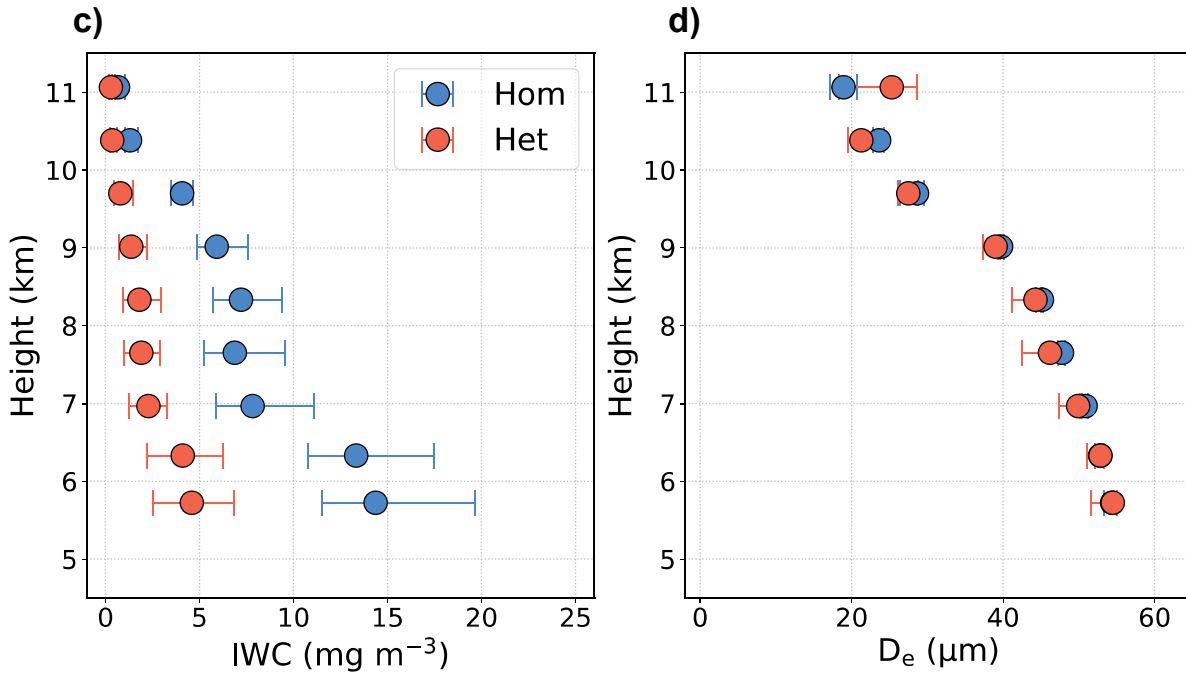
250 Figure 2. Vertical profiles of a) temperature and b) water mixing ratio for wintertime. The libRadtran RTM standard profiles are for subarctic (no Arctic/Antarctic profile provided), whereas MERRA2 profiles are for the Arctic region (60-90°N) during the boreal winter of 2008, 2010, 2012, and 2013. Mean refers to area-weighted average over all grid points in this region.

**Arctic, DJF  
Land**



255

**Ocean**



260

Figure 3. Microphysical properties of cirrus clouds from CALIPSO retrievals: a&c) IWC vs. height and b&d)  $D_e$  vs. height for two cirrus regimes (homogeneous and heterogeneous). The results are for Arctic (60-90°N) during boreal winter (DJF) of 2008, 2010, 2012, and 2013 and for two different surface types: a-b) land and c-d) ocean. Markers show median values, whereas error bars show 25<sup>th</sup> and 75<sup>th</sup> percentiles.

numerous cirrus cloud samples for various heights, grid points, and days, and therefore, it is not correct to assume that it represents a single cirrus from the lowest to highest height shown. For 265 practical purposes, the IWC and  $D_e$  apparent "profiles" from the lowest to highest height for each cirrus regime are divided into 4 clouds each having a thickness of  $\sim 1.3$  km (Dowling and Radke, 1990; Gouveia et al., 2017), but with different cloud base and top heights (CBHs and CTHs). Each of these clouds with their respective IWC and  $D_e$  profiles (with an approximate vertical resolution of 50 m) are then used as input to an RTM to simulate the radiative properties for that cloud.

## 270 2.2 Radiative Transfer Model (RTM)

In this study, the calculations of various thermal or LW fluxes and solar or SW fluxes are conducted using an RTM termed library for Radiative transfer (libRadtran), which employs "uvspec" as its main core (Emde et al., 2016). For simplicity, we refer to libRadtran uvspec as 275 RTM in the rest of this paper. The RTM solver is selected to be the one-dimensional Discrete Ordinate Radiative Transfer model (DISORT; Stamnes et al., 2000; Buras et al., 2011) with six streams. The spectral wavelength range is from 0.25  $\mu\text{m}$  to 5  $\mu\text{m}$  for SW and from 3.1  $\mu\text{m}$  to 100  $\mu\text{m}$  for LW radiation. In addition, the REPTRAN parameterization with fine resolution is selected to account for molecular absorption (Gasteiger et al., 2014).

The RTM has the option to calculate the radiative impact of clouds based on the vertical profiles 280 of cloud water content and effective radius ( $r_e$ ) which are provided as inputs. Ice and liquid cloud properties need to be specified separately in the RTM input files. To calculate the cloud optical properties from IWC and  $r_e$  in the RTM, we specify the Baum parameterization (Baum et al., 2005) with the assumption of a general habit mixture (GHM). The GHM consists of a mixture of different 285 ice particle shapes or habits (e.g. columns, plates, bullet rosettes, aggregates) that vary with particle size. This allows for a more realistic representation of the ice particles since cirrus clouds consist of a wide range of ice habits and sizes (Erfani and Mitchell, 2016, 2017; Lawson et al., 2019). The liquid cloud parameterization of RTM follows the method of Hu and Stamnes (1993). The preparation of variables required for the atmospheric profile file is explained in Sect. 2.1.

By turning on the aerosols option in the RTM, we select the fall-winter season and the maritime 290 haze for the atmosphere below 2 km (as boundary layer or BL) and the background for the

atmosphere above 2 km (as free troposphere or FT), following the aerosol model of Shettle (1989) for the main RTM simulations. The broadband thermal emissivity ( $\varepsilon$ ) varies based on the surface type. Although the  $\varepsilon$  value of snow and ice surfaces is very close to that of a blackbody (equal to unity), it is approximately 0.99 for ocean and forest, and lower for surface types such as cropland, shrubland, and deserts (Wilber et al., 1999). Nonetheless, the sensitivity of LW fluxes to  $\varepsilon$  is much smaller than that to temperature based on Stefan–Boltzmann law. Therefore, we use an  $\varepsilon$  value of unity throughout this study but conduct simulations to investigate the sensitivity to temperature.

A summary of RTM experiments in this study is provided in Table 1. A total of 220 simulations are conducted for various regions (Arctic, Antarctic, NH midlatitude), surface type (land and ocean), and different upper-level cloud conditions (homogeneous, heterogeneous, and clear sky). Furthermore, we explore sensitivity to low liquid clouds, thermodynamic profiles, and atmospheric aerosols. In order to test the impact of low liquid cloud, we add a layer from 500 m to 1100 m

Table 1. A summary of RTM runs conducted in this study.

Experiment	Region	Season	Surface type	Radiation	Cirrus cloud regimes	Number of simulations
Main runs using CALIPSO IWC and $D_e$ (median, upper quartile, and lower quartile profiles)	Arctic	DJF	Land	LW	Hom, Het, Clr	25
	Arctic	DJF	Ocean	LW	Hom, Het, Clr	24
	Antarctic	JJA	Land	LW	Hom, Het, Clr	25
	Antarctic	JJA	Ocean	LW	Hom, Het, Clr	24
	NH midlatitude	DJF	Land	LW	Hom, Het, Clr	25
	NH midlatitude	DJF	Land	SW	Hom, Het, Clr	25
Sensitivity to meteorology (min and max $T$ and $q_v$ profiles)	Arctic	DJF	Land	LW	Hom, Het, Clr	16
Sensitivity to low clouds (with three LWC values)	Arctic	DJF	Land	LW	Hom, Het, Clr	24
Sensitivity to aerosols (two BL and two FT options)	Arctic	DJF	Land	LW	Hom, Het, Clr	32
						<b>Total: 220</b>

305 (thickness of 600 m) with cloud droplet  $r_e$  of 7  $\mu\text{m}$ . These values are consistent with field measurements of low clouds over the Arctic Ocean and Greenland (Järvinen et al., 2023). Three low liquid clouds are tested by varying liquid water content (LWC): 0.01, 0.03, and 0.05  $\text{g m}^{-3}$ . To investigate the effect of thermodynamic profiles, we use the maximum and minimum  $T$  and  $q_v$  profiles in the Arctic during the winter (Fig. 2) and conduct RTM sensitivity tests. Also, four 310 different aerosol options are explored for RTM sensitivity to aerosols: “marine haze, low volcanic”, “urban haze, low volcanic”, “marine haze, high volcanic”, and “urban haze, high volcanic”.

### 2.3 Cloud Radiative Effect

315 The change in radiative fluxes caused by cirrus clouds is quantified by the CRE following Loeb et al. (2009):

$$\text{CRE}_{\text{LW}_z} = (\text{LW} \downarrow_{z_{\text{cld}}} - \text{LW} \uparrow_{z_{\text{cld}}}) - (\text{LW} \downarrow_{z_{\text{clr}}} - \text{LW} \uparrow_{z_{\text{clr}}}), \quad (1)$$

320 where  $z$  refers to a specific height (which is either TOA or Sfc in this study], arrows indicate upward or downward fluxes, “cld” refers to the cloudy condition, and “clr” refers to the clear-sky condition. Each term is in units of  $\text{W m}^{-2}$  and all the radiative fluxes in the right-hand side of the above equation are the outputs of the RTM. As shown in Eq. (1), we consider downward fluxes as positive and vice versa throughout this study. The CRE in the Atm is calculated as:

$$\text{CRE}_{\text{LW}_{\text{Atm}}} = \text{CRE}_{\text{LW}_{\text{TOA}}} - \text{CRE}_{\text{LW}_{\text{Sfc}}}. \quad (2)$$

325 A similar set of equations is used to derive the SW CRE. In our RTM study, we use  $\text{CRE}_{\text{LW}_{\text{Sfc}}}$  to estimate the instantaneous effect of cirrus clouds, while  $\text{CRE}_{\text{LW}_{\text{Atm}}}$  represents the cirrus effect that could potentially influence the surface over longer timescales through adjustment and feedback processes. The net CRE is defined as:

$$\text{CRE}_{\text{net}_z} = \text{CRE}_{\text{LW}_z} + \text{CRE}_{\text{SW}_z}, \quad (3)$$

330 which can be calculated for the TOA, Sfc, or Atm. In this study, we define CCT as the transition from homogeneous to heterogeneous cirrus and calculate its efficacy,  $\Delta\text{CRE}$ , as the difference in CRE between homogeneous and heterogeneous:

$$\Delta\text{CRE} = \langle \text{CRE}_{\text{net}_z, \text{het}} - \text{CRE}_{\text{net}_z, \text{hom}} \rangle, \quad (4)$$

where angle brackets show the average for the four cirrus clouds at 4 different altitudes, as explained in Sect. 2.1. Note that  $\Delta\text{CRE}$  is based on the ideal assumptions that cirrus cloud overcast condition exists. Therefore, correction factors are required to estimate a more realistic impact:

335  $\Delta\text{CRE}_{\text{max}} = \Delta\text{CRE} \times \text{CF}_{\text{cirrus}} \times F_{\text{hom}},$  (5)

where  $\Delta\text{CRE}_{\text{max}}$  indicates that new cirrus cloud formation is not accounted for, and  $\text{CF}_{\text{cirrus}}$  is cirrus cloud fraction and  $F_{\text{hom}}$  is fraction of homogeneous cirrus clouds. The CALIPSO cirrus cloud analysis of Mitchell and Garnier (2024) does not explicitly provide values of  $\text{CF}_{\text{cirrus}}$ .

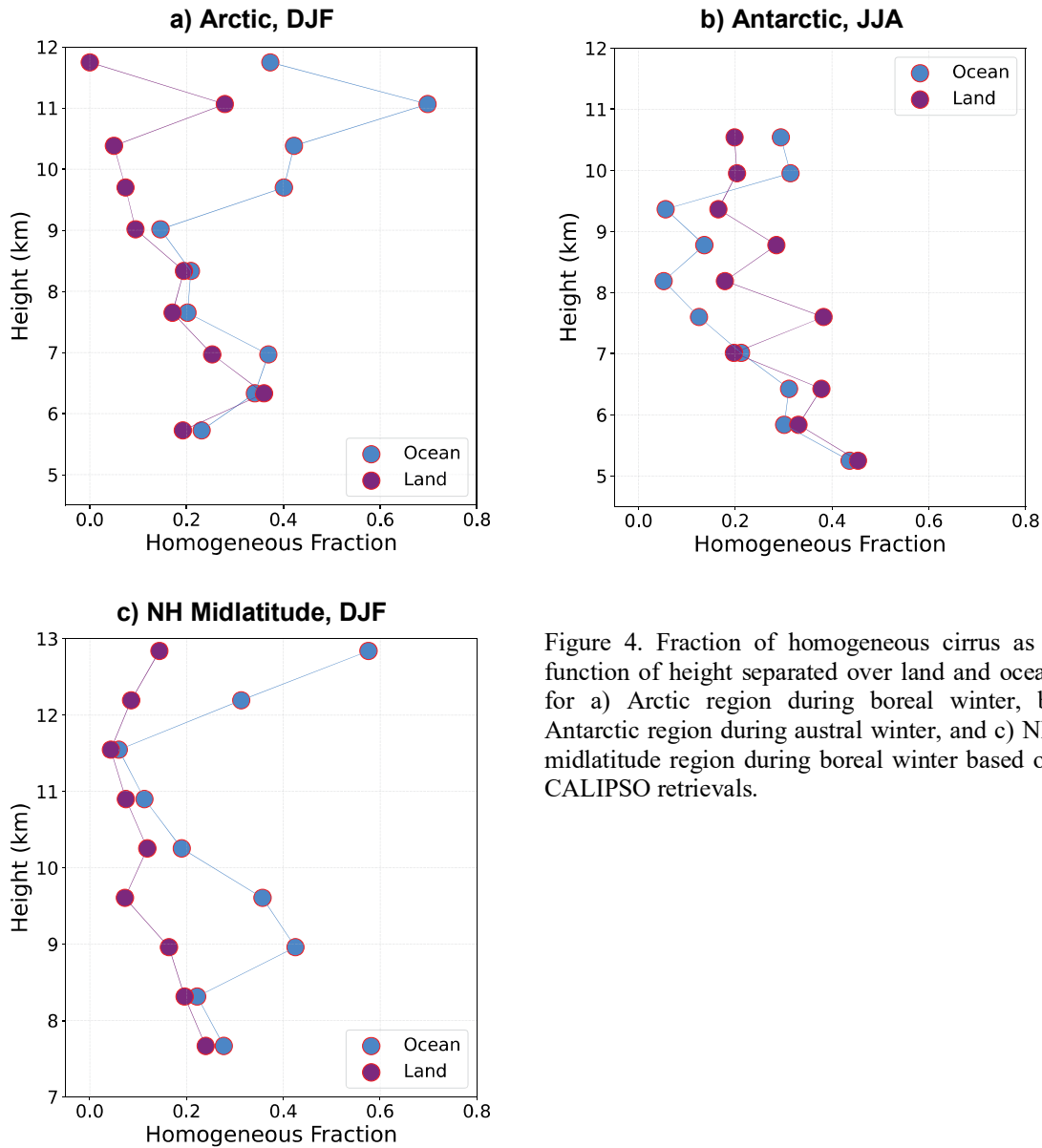


Figure 4. Fraction of homogeneous cirrus as a function of height separated over land and ocean for a) Arctic region during boreal winter, b) Antarctic region during austral winter, and c) NH midlatitude region during boreal winter based on CALIPSO retrievals.

340 Therefore, we use a typical value of 35% for extratropical regions (Gasparini et al., 2023). This estimate may be conservative for the polar regions during winter when ice cloud coverage is greater than in other seasons (Hong et al., 2016; Mitchell et al., 2018; Sassen et al., 2009). The retrievals provide vertical profiles of the homogeneous fraction (defined as the number of homogeneous cirrus pixels divided by the total number of cirrus pixels) for different regions and  
 345 seasons as shown in Fig. 4. Strong variability is seen in homogeneous fraction with height, region (Arctic, Antarctic, and midlatitude), and surface type (land and ocean) and this makes it important to conduct a different RTM simulation for each of those geographical conditions. We use the IWC-weighted average of the homogeneous fraction to calculate  $F_{\text{hom}}$ . In this study, Sfc  $\Delta\text{CRE}_{\text{max}}$  is used to estimate the instantaneous efficacy of CCT, while Atm  $\Delta\text{CRE}_{\text{max}}$  represents the potential  
 350 CCT effect—that is, the extent to which changes in atmospheric heating due to CCT could ultimately influence the surface through climatic feedback processes.

Note that  $\Delta\text{CRE}_{\text{max}}$  emphasizes the first CCT scenario, namely the transition from homogeneous cirrus to heterogeneous cirrus. To account for new cirrus clouds formed by INPs injected into clear-sky ice-supersaturated regions, we only consider the heterogeneous cirrus CRE, because  
 355 homogeneous cirrus clouds depend primarily on  $\text{RH}_i$  and would form regardless. As mentioned, Lin et al. (2025) and Sporre et al. (2022) report that elevated INP concentrations within volcanic plumes entering the troposphere increased the cirrus coverage or fraction by approximately 20% (denoted here as  $\Delta\text{CF}_{\text{new cirrus}}$ ). This provides a means of estimating the CRE of new cirrus:

$$\text{CRE}_{\text{new cirrus}} = \Delta\text{CF}_{\text{new cirrus}} \times \text{CF}_{\text{cirrus}} \times \langle \text{CRE}_{\text{netz,het}} \rangle. \quad (6)$$

360 Finally, the total  $\Delta\text{CRE}$  can be calculated as:

$$\Delta\text{CRE}_{\text{tot}} = \Delta\text{CRE}_{\text{max}} + \text{CRE}_{\text{new cirrus}}. \quad (7)$$

### 3 Main RTM simulations

#### 3.1 Arctic region

365 The RTM simulations are conducted using mean thermodynamic profiles from MERRA2 for the Arctic during the boreal winter (Fig. 2) and ice cloud properties using the median, 25<sup>th</sup> and 75<sup>th</sup> percentile IWC and  $D_e$  from CALIPSO satellite retrievals, as shown in Fig. 3. A general pattern of

370 cirrus cloud properties is seen in Fig. 3 (e.g., a decrease in both IWC and  $D_e$  with height, which is characteristic of cirrus clouds). The difference in IWC between homogeneous and heterogeneous  
370 cirrus is distinct, as homogeneous cirrus in our CALIPSO retrievals have much larger IWC than heterogeneous cirrus at the same temperature, in agreement with previous observational studies conducted over Europe and Africa (Krämer et al., 2016, 2020) and over the Americas and Pacific Ocean (Ngo et al., 2024; Patnaude et al., 2021; Patnaude and Diao, 2020). Mitchell et al. (2024) showed that the CALIPSO retrievals generally agree well with aircraft measurements from Krämer  
375 et al. (2020). See the former for a more detailed discussion on the similarities and differences between satellite and aircraft-based observation techniques.

380 Despite the distinct pattern in IWC among homogeneous and heterogeneous cirrus,  $D_e$  values are similar in both cirrus regimes, which results from the criteria applied to define heterogeneous and homogeneous cirrus clouds in Mitchell and Garnier (2024). That is, when  $D_e$  is plotted against either the SW  $\alpha_{ext}$  or IWC as shown in Fig. S1, there is generally a  $D_e$  maximum that divides the two cirrus regimes for a given  $T$ . The maximum in the number of CALIPSO cirrus cloud samples when related to  $\alpha_{ext}$  or IWC tends to coincide with this  $D_e$  maximum, resulting in similar mean  $D_e$  values for each cirrus regime. But as  $\alpha_{ext}$  or IWC increases beyond this  $D_e$  maximum,  $D_e$  decreases, which is consistent with conventional knowledge that an increase in homogeneous ice nucleation  
385 activity will act to increase  $N_i$  and decrease particle sizes due to water vapor competition effects.

390 Due to different cloud properties over land and ocean, different RTM simulations are conducted for land and ocean. Figure 5 shows TOA, Sfc, and Atm LW CRE calculated from RTM simulations using Eqs. (1) and (2). Note that no RTM simulation is conducted for SW range because of the absence of solar radiation in this region during the winter. As such, these results serve as net CRE (Eq. 3). LW CRE in Fig. 5 varies with CBH, highlighting the effects of cirrus cloud altitude as well as microphysical properties. The LW CRE at the surface generally decreases with CBH because colder clouds at higher altitudes emit less LW radiation compared to warmer clouds at lower altitudes, based on the Stefan–Boltzmann law. Note that cirrus cloud altitude is closely related to cirrus cloud temperature, since both are connected via the vertical temperature profile.  
395 In addition, cirrus clouds at higher altitudes often have lower IWC (Fig. 3), and this makes them optically thinner. In contrast, smaller  $D_e$  in cirrus at higher altitudes could lead to stronger LW CRE (Fu and Liou, 1993). At the TOA, LW CRE depends on the difference between the cloud's

LW emission and the emission from the Earth's surface (Corti and Peter, 2009), and such difference is larger for cirrus at higher altitudes.

400 Also seen in Fig. 5 is significantly larger LW CRE at the TOA, at the Sfc, and within the Atm for homogeneous cirrus than that for heterogeneous cirrus of the same altitude. This is mainly due to higher IWC values for homogeneous cirrus (Fig. 3), which leads to optically thicker cirrus (Krämer et al., 2016, 2020). When both cirrus regimes have comparable IWC, as seen for the highest

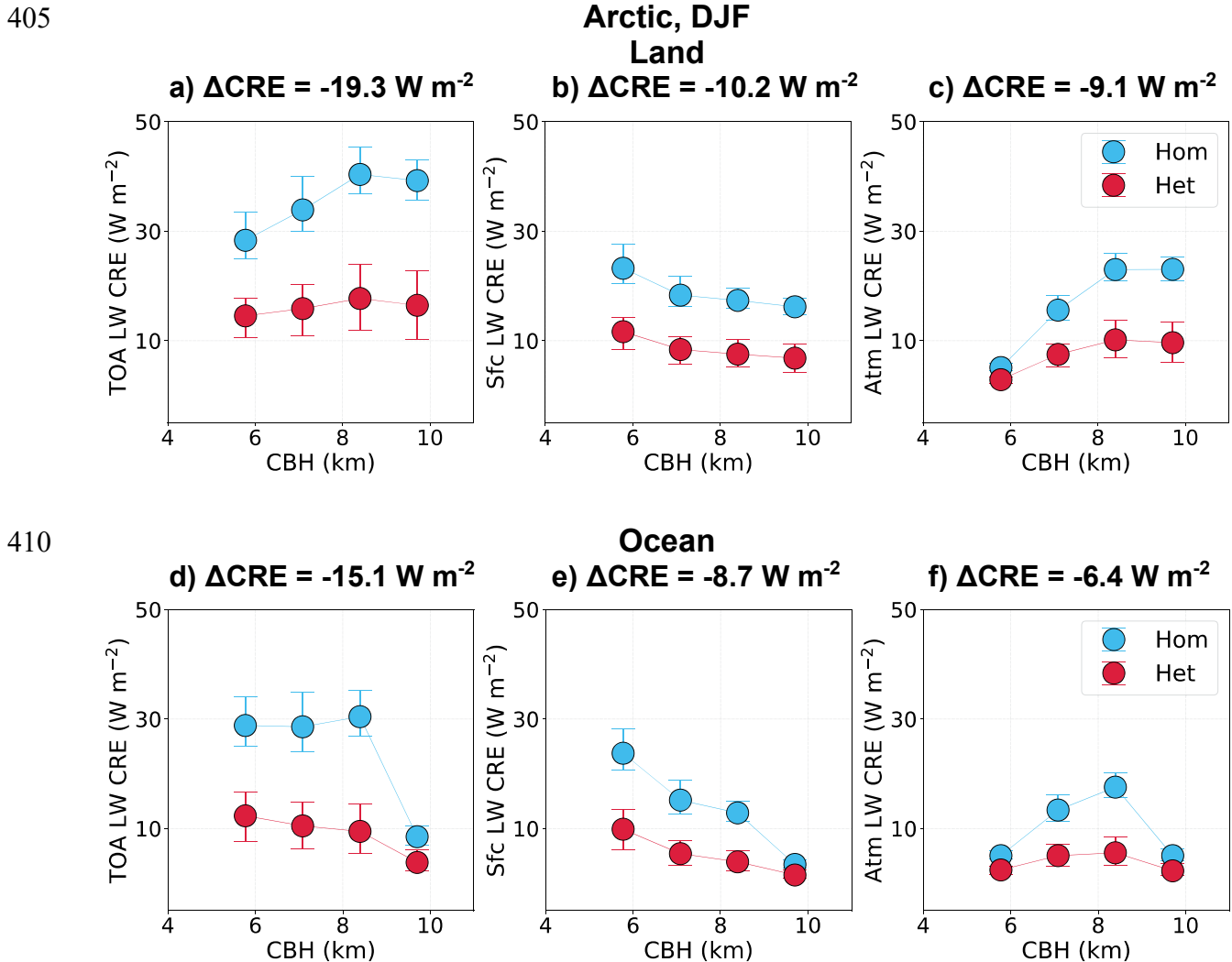


Figure 5. Results of RTM simulations showing LW CRE as a function of CBH over the Arctic during the boreal winter for 4 cirrus clouds separated based on surface types (land and ocean) and cirrus regimes (homogeneous and heterogeneous). The CRE is calculated at the TOA, at the surface, and within the column of atmosphere. The  $\Delta\text{CRE}$  at the top of each panel represent the transition from homogeneous to heterogeneous cirrus based on Eq. (5). A total of 48 RTM simulations are shown in this figure with markers and error bars referring to simulations based on CALIPSO profiles in Fig. 4.

420 altitude over the ocean, their LW CRE is comparable. This highlights the critical role of IWC in determining the radiative impact of cirrus clouds.

Over land, the CCT efficacy, defined as the transition from homogeneous to heterogeneous cirrus and quantified by  $\Delta\text{CRE}$  in Eq. (4), results in a TOA cooling effect of  $-19.3 \text{ W m}^{-2}$  (the mean value of the four clouds considered), with a corresponding Sfc cooling of  $-10.2 \text{ W m}^{-2}$  and atmospheric column cooling of  $-9.1 \text{ W m}^{-2}$  (Figs. 5a-c). Considering that the typical cirrus cloud cover over the Arctic is 35% and that the IWC-weighted average of the homogeneous fraction is 0.21 (Fig. 4a), Eq. 5 gives the maximum cooling effect  $\Delta\text{CRE}_{\text{max}}$  at the TOA, Sfc, and Atm as  $\sim -1.4$ ,  $-0.7$ , and  $-0.7 \text{ W m}^{-2}$ , respectively (Table 2). Consequently, after accounting for the impact of new cirrus formation, the total cooling effect  $\Delta\text{CRE}_{\text{tot}}$  at the TOA, Sfc, and Atm is  $\sim -0.3$ ,  $-0.2$ , and  $-0.1 \text{ W m}^{-2}$ , respectively. Of particular importance for CCT is the cooling at the surface but note that the RTM provides instantaneous values. For the atmospheric column, the RTM calculates a cooling effect that is similar to the surface cooling. This might have implications for long-term feedback processes and possibly impact of AA, as the atmospheric column cooling could lead to lower geopotential thickness over the Arctic, which in turn might affect meridional  $T$  gradients, thermal winds, and the extratropical jet stream (Cohen et al., 2020). However, a careful GCM study is required to test this hypothesis.

The overall pattern of cooling over the ocean is consistent with that over land, but the cooling effect over the ocean is slightly weaker, with a TOA  $\Delta\text{CRE}$  of  $-15.1$ , a Sfc  $\Delta\text{CRE}$  of  $-8.7 \text{ W m}^{-2}$  and an Atm  $\Delta\text{CRE}$  of  $-6.4 \text{ W m}^{-2}$  (Figs. 5d-f). With a typical cirrus cloud cover value of 35% and IWC-weighted mean homogeneous fraction of 0.29 (Fig. 4a) over the ocean, TOA, Sfc, and Atm  $\Delta\text{CRE}_{\text{max}}$  are approximately  $-1.5$ ,  $-0.9$ , and  $-0.6 \text{ W m}^{-2}$ , respectively (Table 2). These values are higher than  $\Delta\text{CRE}_{\text{max}}$  over land because of the higher homogeneous fraction over the ocean. In addition, TOA, Sfc, and Atm  $\Delta\text{CRE}_{\text{tot}}$  are  $\sim -0.9$ ,  $-0.5$ , and  $-0.4 \text{ W m}^{-2}$ , respectively. Note that in Mitchell and Garnier (2024), regions consisting of sea ice are considered as land. As shown in Fig. 445 S2a, the higher sea ice fraction in winter along with the pure land fraction constitutes a much larger area than water surfaces. As such,  $\Delta\text{CRE}_{\text{tot}}$  over the ocean makes a smaller impact. Nevertheless, we conduct analysis for both land and ocean for a more comprehensive analysis.

### 3.2 Antarctic region

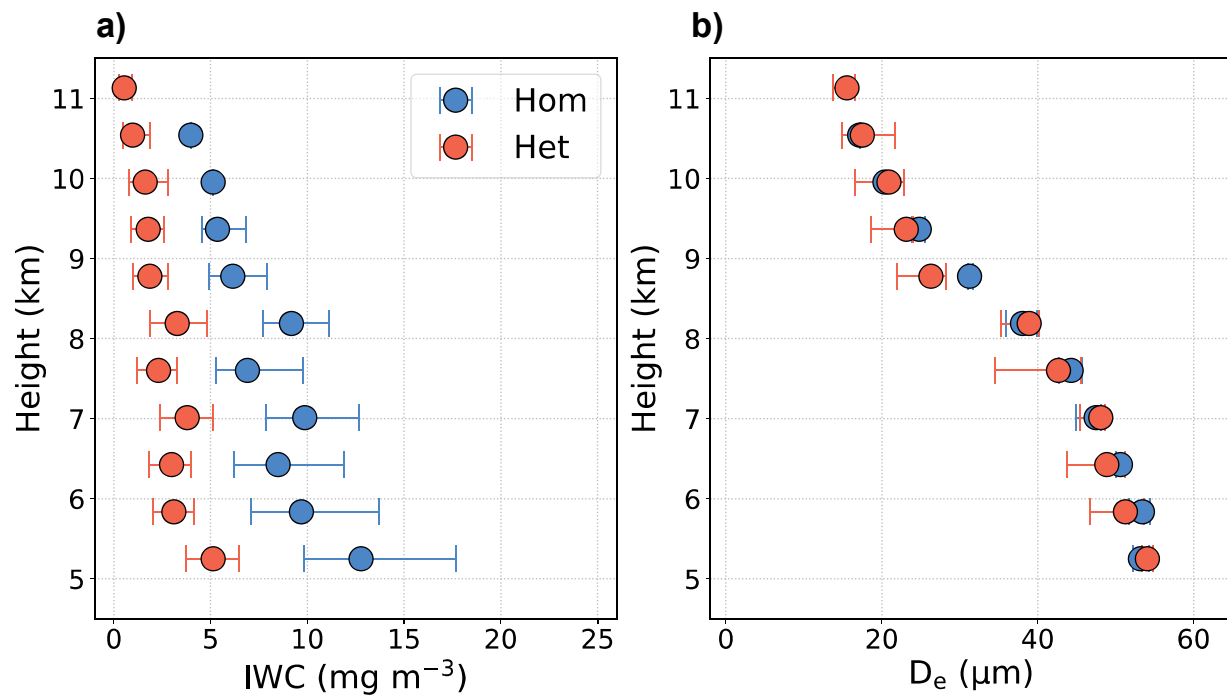
The RTM simulations for the Antarctic are conducted similarly to those for the Arctic, using mean  
450 thermodynamic profiles from MERRA2 (not shown) and median, 25<sup>th</sup> and 75<sup>th</sup> percentile IWC and  
*D<sub>e</sub>* profiles from CALIPSO satellite retrievals (Fig. 6) during the austral winter for this region. While the general patterns of IWC and *D<sub>e</sub>* profiles for homogeneous and heterogeneous cirrus are similar to those in the Arctic, the specific values and details differ between the two regions. Simulations are performed for both land and ocean, and the LW CRE (equivalent to net CRE due  
455 to the absence of SW radiation during austral winter) is calculated at the TOA, Sfc, and Atm, as shown in Fig. 7.

The TOA CRE over Antarctic land is weaker than that over the Arctic for cirrus clouds at the same altitude, particularly for homogeneous cirrus at the two lowest altitudes. This is likely due to lower IWC in the lowest altitudes over the Antarctic compared to the Arctic (Figs. 3 and 6). As a result,  
460 the transition from homogeneous to heterogeneous cirrus, quantified by  $\Delta\text{CRE}$ , leads to a TOA cooling of  $-15.4 \text{ W m}^{-2}$ , which is roughly 20% weaker than the  $\Delta\text{CRE}$  over Arctic land. The Sfc and Atm  $\Delta\text{CRE}$  values are  $-9.2 \text{ W m}^{-2}$  ( $\sim 10\%$  weaker than that over the Arctic land), and  $-6.2 \text{ W m}^{-2}$  ( $\sim 40\%$  weaker than that over the Arctic land), respectively. Despite the lower IWC for homogeneous cirrus over the Antarctic, the homogeneous fraction is significantly higher (IWC-weighted average is 0.30), resulting in stronger maximum cooling over the Antarctic land than over the Arctic land; the maximum cooling effects ( $\Delta\text{CRE}_{\text{max}}$ ) at the TOA, Sfc, and Atm are approximately  $-1.6$ ,  $-1.0$ , and  $-0.6 \text{ W m}^{-2}$ , respectively, and the total cooling effects ( $\Delta\text{CRE}_{\text{tot}}$ ) at the TOA, Sfc, and Atm are  $\sim -0.7$ ,  $-0.4$ , and  $-0.3 \text{ W m}^{-2}$ , respectively (Table 2).  
465

470 Table 2. Quantifying the transition from homogeneous to heterogeneous cirrus (for overcast skies) using the change in their cloud radiative effect ( $\Delta\text{CRE}$ ) and its maximum value that assumes 35% cloud coverage ( $\Delta\text{CRE}_{\text{max}}$ ) at various levels based on Eq. (5) for different regions, seasons, and surface types. In addition, total values ( $\Delta\text{CRE}_{\text{tot}}$ ) are provided based on Eq. (7) to account for the new cirrus formation.

Region	Season	Surface type	$F_{\text{hom}}$	$\Delta\text{CRE} (\text{W m}^{-2})$			$\Delta\text{CRE}_{\text{max}} (\text{W m}^{-2})$			$\Delta\text{CRE}_{\text{tot}} (\text{W m}^{-2})$		
				TOA	Sfc	Atm	TOA	Sfc	Atm	TOA	Sfc	Atm
Arctic	DJF	Land	0.21	-19.3	-10.2	-9.1	-1.4	-0.7	-0.7	-0.3	-0.2	-0.1
		Ocean	0.29	-15.1	-8.7	-6.4	-1.5	-0.9	-0.6	-0.9	-0.5	-0.4
Antarctic	JJA	Land	0.3	-15.4	-9.2	-6.2	-1.6	-1.0	-0.6	-0.7	-0.4	-0.3
		Ocean	0.24	-13.7	-9.3	-4.3	-1.2	-0.8	-0.4	-0.5	-0.3	-0.2
NH midlat	DJF	Land	0.15	-22.9	+0.2	-23.1	-1.2	0.0	-1.2	+0.3	+0.0	+0.3

**Antarctic, JJA**  
**Land**



**Ocean**

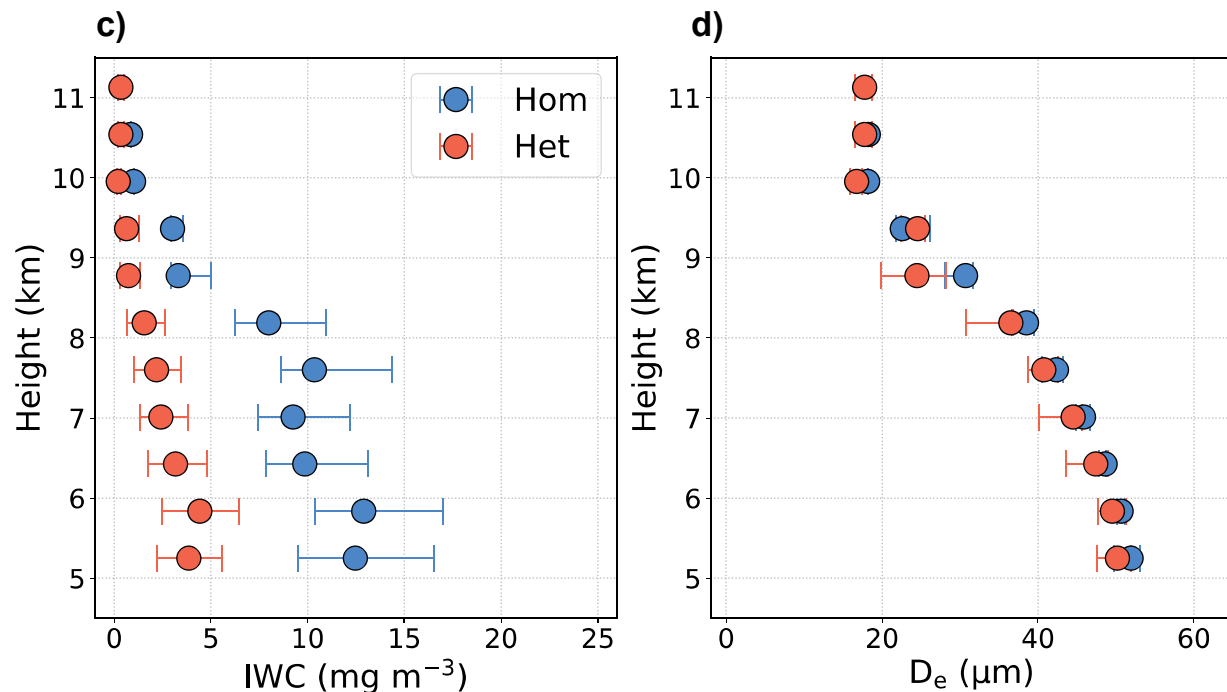
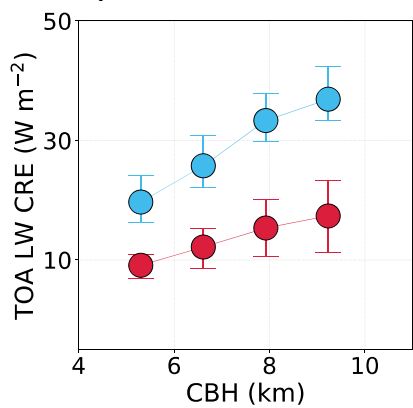


Figure 6. As in Fig. 3, but the results are for Antarctic (90-60°S) during austral winter (JJA).

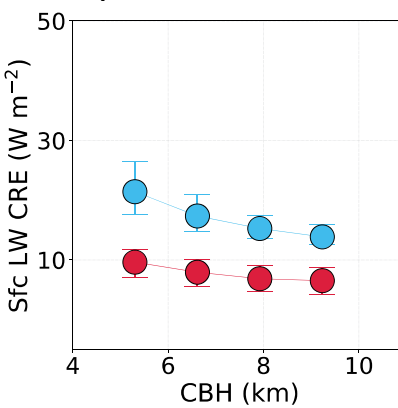
**Antarctic, JJA**

**Land**

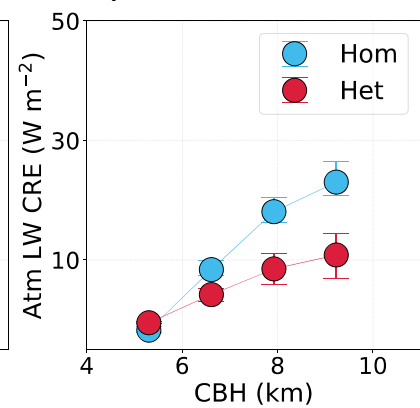
**a)  $\Delta\text{CRE} = -15.4 \text{ W m}^{-2}$**



**b)  $\Delta\text{CRE} = -9.2 \text{ W m}^{-2}$**



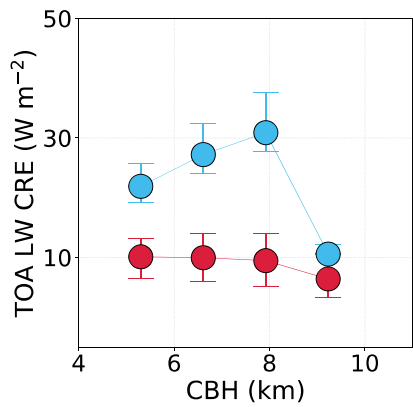
**c)  $\Delta\text{CRE} = -6.2 \text{ W m}^{-2}$**



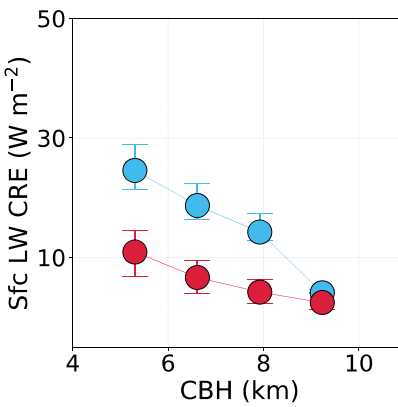
490

**Ocean**

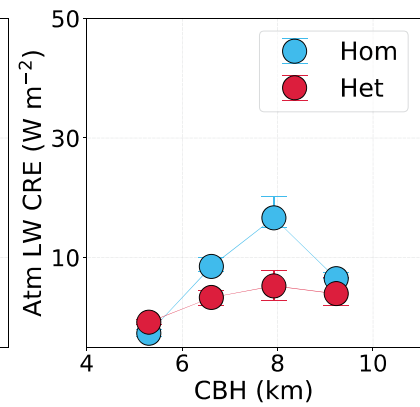
**d)  $\Delta\text{CRE} = -13.7 \text{ W m}^{-2}$**



**e)  $\Delta\text{CRE} = -9.3 \text{ W m}^{-2}$**



**f)  $\Delta\text{CRE} = -4.3 \text{ W m}^{-2}$**



495

Figure 7. As in Fig. 5, but the results are RTM simulations for Antarctic during austral winter.

Over the ocean, the TOA cooling effect ( $\Delta\text{CRE}$ ) is weaker compared to all previous results in this study. The TOA, Sfc, and Atm  $\Delta\text{CRE}$  values are estimated to be  $-13.7$ ,  $-9.3$ , and  $-4.3 \text{ W m}^{-2}$ , respectively. With an IWC-weighted average homogeneous fraction of 0.24,  $\Delta\text{CRE}_{\text{max}}$  at the TOA, Sfc, and Atm are approximately  $-1.2$ ,  $-0.8$ , and  $-0.4 \text{ W m}^{-2}$ , respectively, and  $\Delta\text{CRE}_{\text{tot}}$  at the TOA, Sfc, and Atm are  $\sim -0.5$ ,  $-0.3$ , and  $-0.2 \text{ W m}^{-2}$ , respectively (Table 2). These values are weaker than those for Antarctic land and Arctic ocean. However, for the Antarctic, the CCT cooling effect over the ocean is much smaller than that over land, given that the surface water fraction is much smaller than the fraction of sea ice and the Antarctic land mass during austral winter (Fig. S2b).

To the best of our knowledge, no previous study has used an RTM to estimate the cooling efficacy of CCT. Although the instantaneous surface cooling in our study for both polar regions and over land and ocean (Sfc  $\Delta\text{CRE}_{\text{max}}$ : -0.7 to -1.0  $\text{W m}^{-2}$  and Sfc  $\Delta\text{CRE}_{\text{tot}}$ : -0.2 to -0.5  $\text{W m}^{-2}$ ) and the 510 TOA cooling (TOA  $\Delta\text{CRE}_{\text{max}}$ : -1.2 to -1.6  $\text{W m}^{-2}$  and TOA  $\Delta\text{CRE}_{\text{tot}}$ : -0.3 to -0.9  $\text{W m}^{-2}$ ) are much weaker than the potential cooling of -2.8  $\text{W m}^{-2}$  suggested by Mitchell and Finnegan (2009), they fall within the range of maximum CCT cooling from previous GCM studies, from -0.25  $\text{W m}^{-2}$  515 (Gasparini and Lohmann, 2016) to -2  $\text{W m}^{-2}$  (Storelvmo et al., 2013; Storelvmo and Herger, 2014). We acknowledge that this is not a direct comparison, as GCMs calculate global CREs while 520 accounting for feedback processes. However, we note that CCT in the polar regions during winter could be as effective as CCT applied globally throughout the year, as the significant LW trapping by cirrus clouds outside the polar regions is counteracted by SW scattering (Storelvmo et al., 2014).

### 3.3 North hemispheric mid-latitude region

Mid-latitude regions ( $30^{\circ}\text{N}$  to  $60^{\circ}\text{N}$  and  $-60^{\circ}\text{S}$  to  $-30^{\circ}\text{S}$  latitude bands) comprise 520 approximately 37% of the Earth's surface, which is about three times the area of the high latitudes. This makes it important to evaluate the potential efficacy of CCT in these regions. During winter, the SW impact of cirrus clouds is minimized due to shorter days and higher solar zenith angles (SZA). The SZA, which is the angle between the Sun's rays and a line perpendicular to the Earth's 525 surface at a specific location (ranging from  $0^{\circ}$  at the equator at midday during an equinox to  $90^{\circ}$  at sunrise and sunset) (Aktaş and Kirçicek, 2021), has a daytime average of  $73^{\circ}$  at  $45^{\circ}\text{N}$  latitude during the winter solstice (Hartmann, 2016). In addition to LW RTM simulations, we conduct SW 530 simulations for a daytime average winter solstice mid-latitude scenario:  $45^{\circ}\text{N}$  latitude, a surface albedo of 0.3, and a SZA of  $73^{\circ}$ . The RTM is forced with mean thermodynamic profiles from MERRA2 (not shown) and median, 25th, and 75th percentile IWC and  $D_e$  profiles from CALIPSO satellite retrievals (Fig. S3) during the boreal winter for NH mid-latitude land.

The results of the RTM simulations for various CREs are shown in Fig. 8. The LW CRE at the TOA over mid-latitudes is significantly larger than that over polar regions for cirrus clouds of the same regime (homogeneous or heterogeneous) and at the same altitude. This is likely due to higher IWC within cirrus clouds (Fig. S3) and a warmer temperature profile for midlatitudes compared 535 to polar regions. Cirrus clouds with higher IWC retain more LW radiation, resulting in stronger

### NH Midlatitude Winter over Land

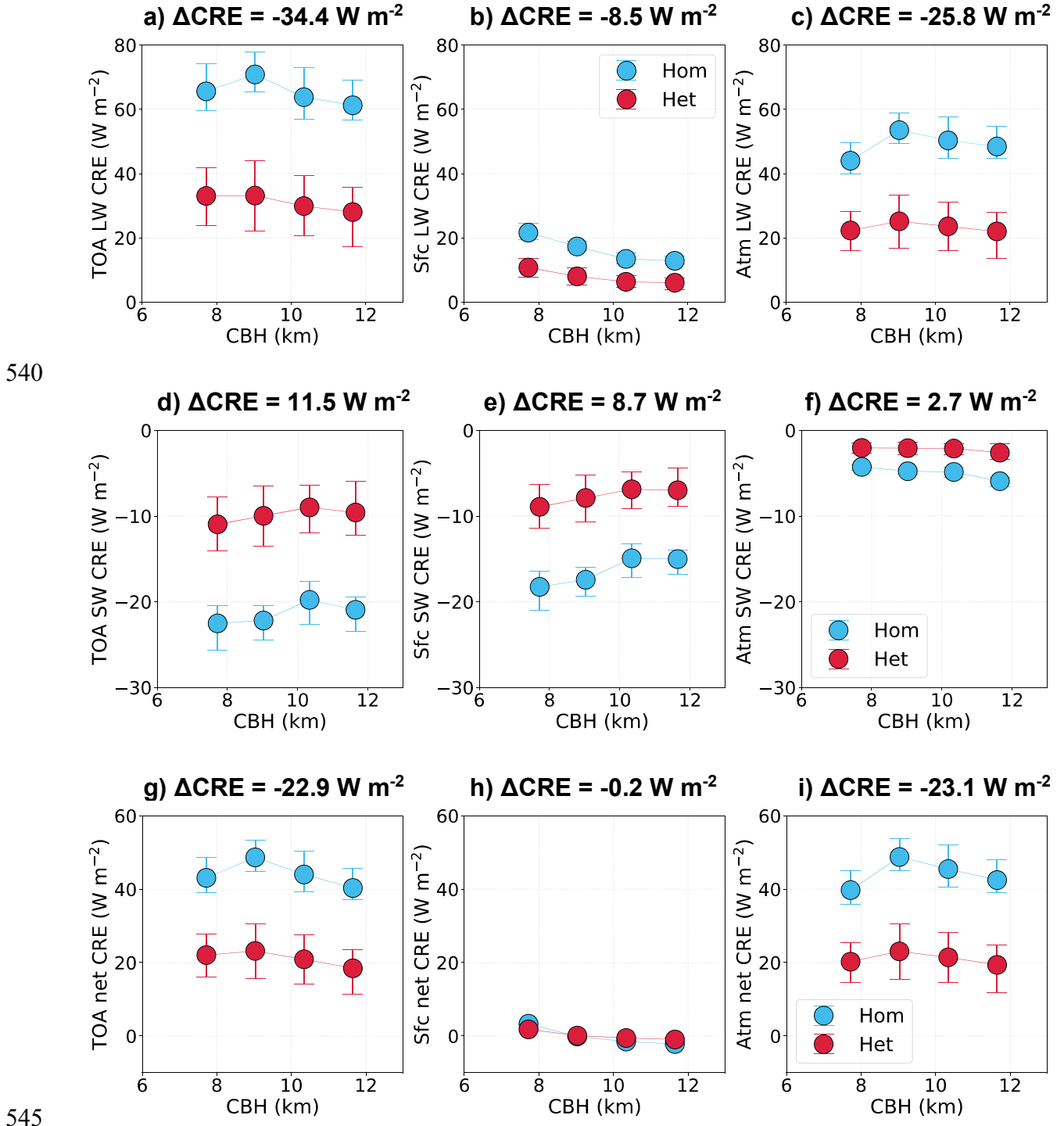


Figure 8. As in Fig. 5, but the results are RTM simulations for LW, SW, and net CRE over NH midlatitude land with a total of 50 RTM simulations.

550 LW CRE (Fu and Liou, 1993). Furthermore, the warmer atmospheric column and in particular warmer surface in mid-latitudes emit more LW radiation toward the upper troposphere, which is absorbed and re-emitted at colder temperatures by cirrus clouds. This causes a stronger difference between LW radiation emitted by cirrus cloud and Earth's surface and enhances the TOA LW CRE (Corti and Peter, 2009).

555 The SW CRE (Figs. 8d–f) is calculated to provide daily-mean values. To account for the diurnal cycle of SW radiation, the SW CRE from Eqs. (1) and (2) is multiplied by a factor of 0.37, representing the ratio of daytime hours (8.8 hours) to 24 hours at 45°N latitude during the winter solstice. This post-simulation factor, combined with the daytime-average SZA used in the RTM simulations, averages the SW CRE at 45°N over a full 24-hour period, consistent with the LW  
560 CRE calculations. All SW CRE values are negative, indicating the cooling effect of cirrus clouds at different altitudes and with various microphysical properties due to the absorption and scattering of solar radiation. Homogeneous cirrus clouds exhibit significantly stronger SW cooling effects than heterogeneous cirrus clouds at the TOA and Sfc, as they contain higher IWC, which corresponds to greater scattering and absorption by ice particles (Fu and Liou, 1993). The change  
565 in SW CRE with cloud altitude depends on changes in  $\alpha_{ext}$ , where  $\alpha_{ext} = 3 \text{ IWC}/(\rho_i D_e)$ , and  $\rho_i$  is bulk density of ice. As cloud altitude increases, both IWC and  $D_e$  decrease, resulting in a relatively slow decrease in  $\alpha_{ext}$  with increasing altitude (Fu and Liou, 1993; Stephens et al., 1990).

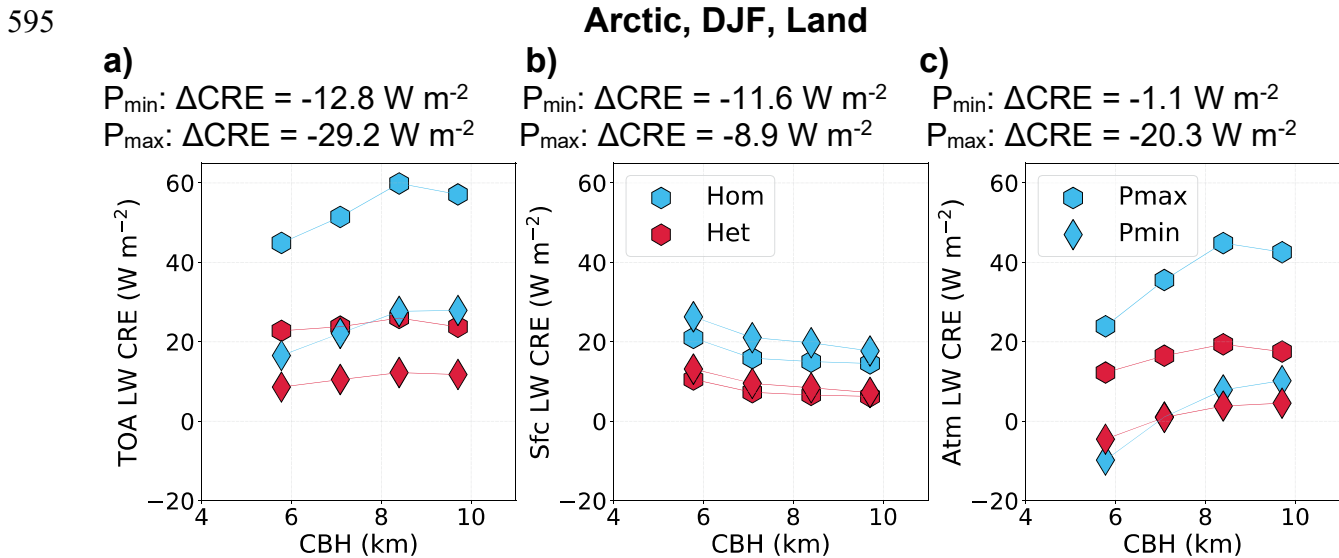
At the TOA, the strong difference in LW CRE between the two regimes results in significant LW cooling ( $\Delta\text{CRE} = -34.4 \text{ W m}^{-2}$ ), which is partially offset by SW warming ( $\Delta\text{CRE} = 11.5 \text{ W m}^{-2}$ ),  
570 yielding a net TOA cooling of  $-22.9 \text{ W m}^{-2}$  (Fig. 8g). The transition from homogeneous to heterogeneous cirrus results in a surface LW cooling ( $\Delta\text{CRE}$ ) of  $-8.5 \text{ W m}^{-2}$ , which is largely offset by SW warming ( $\Delta\text{CRE} = 8.7 \text{ W m}^{-2}$ ), leading to a relatively small net surface  $\Delta\text{CRE}$  of  $-0.2 \text{ W m}^{-2}$  (Fig. 8h). Within the atmospheric column, a significant net cooling of  $-23.1 \text{ W m}^{-2}$  occurs (Fig.  
575 8i). Considering an IWC-weighted average homogeneous fraction of 0.15 (Fig. 4c) and a cirrus cloud cover of 35%, the maximum net cooling effects ( $\Delta\text{CRE}_{\text{max}}$ ) at the TOA, Sfc, and Atm are approximately  $-1.2$ ,  $0.0$ , and  $-1.2 \text{ W m}^{-2}$ , respectively (Table 2). These results demonstrate that in the absence of new cirrus formation, while the instantaneous cooling efficacy of CCT (Sfc net  $\Delta\text{CRE}_{\text{max}}$ ) in mid-latitudes during winter is negligible, CCT could still be effective if its impact on the atmospheric column (Atm net  $\Delta\text{CRE}_{\text{max}}$ ) can reach the surface through feedback processes.

580 However, after accounting for new cirrus formation, the total net effects ( $\Delta\text{CRE}_{\text{tot}}$ ) at the TOA, Sfc, and Atm are  $\sim +0.3$ , 0.0, and  $+0.3 \text{ W m}^{-2}$ , respectively (Table 2), indicating a warming effect and suggesting that CCT could even result in net warming in this season and latitude band.

## 4 Sensitivity tests

### 585 4.1 Sensitivity to thermodynamic profiles

The impact of temperature and humidity on cirrus LW CRE is evaluated using minimum and maximum air  $T$  and  $q_v$  profiles (referred to as  $T_{\min}$  and  $T_{\max}$  for brevity) from MERRA2 data for Arctic land during the winter (Fig. 9). TOA LW CRE significantly increases with an increase in  $T$  and  $q_v$ . In particular, Earth's surface plays an important role because it typically acts as a blackbody (its  $\varepsilon$  is very close to unity), and even a rather small surface warming can significantly enhance LW radiation emitted from the surface, as described by Stefan–Boltzmann law. With unchanged cirrus temperature and LW emission, the enhanced upward LW radiation from the Earth's surface creates a stronger LW contrast, resulting in a stronger TOA LW CRE (Corti and Peter, 2009).



600

Figure 9. Sensitivity of RTM-simulated cirrus CRE to different thermodynamic profiles (P) from MERRA2 minimum and maximum temperature and water mixing ratio (abbreviated as  $P_{\min}$  and  $P_{\max}$ ), as shown in Fig. 2.

At the surface, however, LW CRE is weakly sensitive to thermodynamic profiles (Fig. 9b). Profiles with lower  $T$  and  $q_v$  lead to slightly higher cirrus LW CRE at the surface, particularly for 605 homogeneous cirrus. The surface LW CRE depends primarily on the downward LW radiation from cirrus clouds, rather than surface temperature (Eq. 1). Therefore, the lower surface LW CRE in maximum profiles compared to minimum profiles is due to higher water vapor in the atmosphere, which absorbs part of the downward LW radiation from cirrus clouds before it reaches the surface. This is consistent with the findings of Dupont and Haeffelin (2008).

610 Figure 9a shows that the transition from homogeneous to heterogeneous cirrus ( $\Delta$ CRE) intensifies significantly with warmer and more humid thermodynamic profiles, particularly with higher surface temperatures. The  $\Delta$ CRE for minimum and maximum profiles is  $-12.8 \text{ W m}^{-2}$  and  $-29.2 \text{ W m}^{-2}$ , respectively. At the surface (Fig. 9b), the  $\Delta$ CRE for minimum and maximum profiles is  $-11.6 \text{ W m}^{-2}$  and  $-8.9 \text{ W m}^{-2}$ , respectively, indicating minimal sensitivity to thermodynamic profiles. 615 This consistency suggests that the instantaneous CCT efficacy is robust across different thermodynamic conditions. However, the atmospheric  $\Delta$ CRE (Fig. 9c) shows greater variability, ranging from  $-1.1 \text{ W m}^{-2}$  for the minimum thermodynamic profile to  $-20.3 \text{ W m}^{-2}$  for the maximum profile, highlighting the sensitivity of potential CCT efficacy to thermodynamic profiles.

## 4.2 Sensitivity to Arctic low clouds

620 Low clouds are frequent over the Arctic region and they have a significant impact on the radiation balance (Philipp et al., 2020). These clouds are controlled by many factors including atmospheric circulation and sea ice extent and in return, they impact the sea ice via an ice-albedo feedback (Huang et al., 2021). During the winter, low clouds retain outgoing longwave radiation and warm the surface, but during the summer, this effect is canceled by cooling from reflecting solar radiation 625 (Maillard et al., 2021). Arctic low cloud cover varies by season and this variability is more distinct for higher latitudes of the Arctic (north of latitude 70) where low cloud cover changes from over 50% in summer to lower than 20% in winter (Eastman and Warren, 2010). Arctic low clouds tend to have higher cloud water path (CWP) over the open ocean and lower CWP over ice-covered areas (Yu et al., 2019) due to higher moisture availability over the ocean than ice (Monroe et al., 630 2021). The spatial distribution of arctic low clouds shows that over land their cover is typically around 35% in summer and around 15% in winter. Over the ocean, their cover is around 55% in

summer, but drops below 30% on the Pacific side of the Arctic Ocean, meanwhile remains as high as 50% on the Atlantic side of the Arctic Ocean in winter (Huang et al., 2021).

Our RTM simulations explore the impact of low liquid clouds on cirrus CRE by introducing a low liquid cloud layer, as described in Sect. 2. Three low liquid clouds are tested by varying LWC (e.g., 0.01, 0.03, and 0.05  $\text{g m}^{-3}$ ). To calculate cirrus CRE using Eq. (1), we consider the difference between an RTM run with both cirrus and low liquid cloud versus an RTM run with only low liquid cloud.

The results (Fig. 10) show that TOA LW CRE for cirrus clouds is not sensitive to the low liquid clouds. Over the Arctic, such clouds are close to the surface, and their temperature is very similar to that of the Earth's surface (due to inversion, mean profile of  $T$  in Fig. 2a varies slowly below 2 km). As a result, the LW radiation emitted by low liquid clouds is close to that emitted by Earth's surface. Moreover, we only vary the LWC of low clouds, not their elevation, so their temperature remains constant. Consequently, the difference between cirrus LW radiation and the upward LW radiation from the underlying clouds and Earth's surface does not change significantly across the three sensitivity tests in this section when considering CRE at TOA.

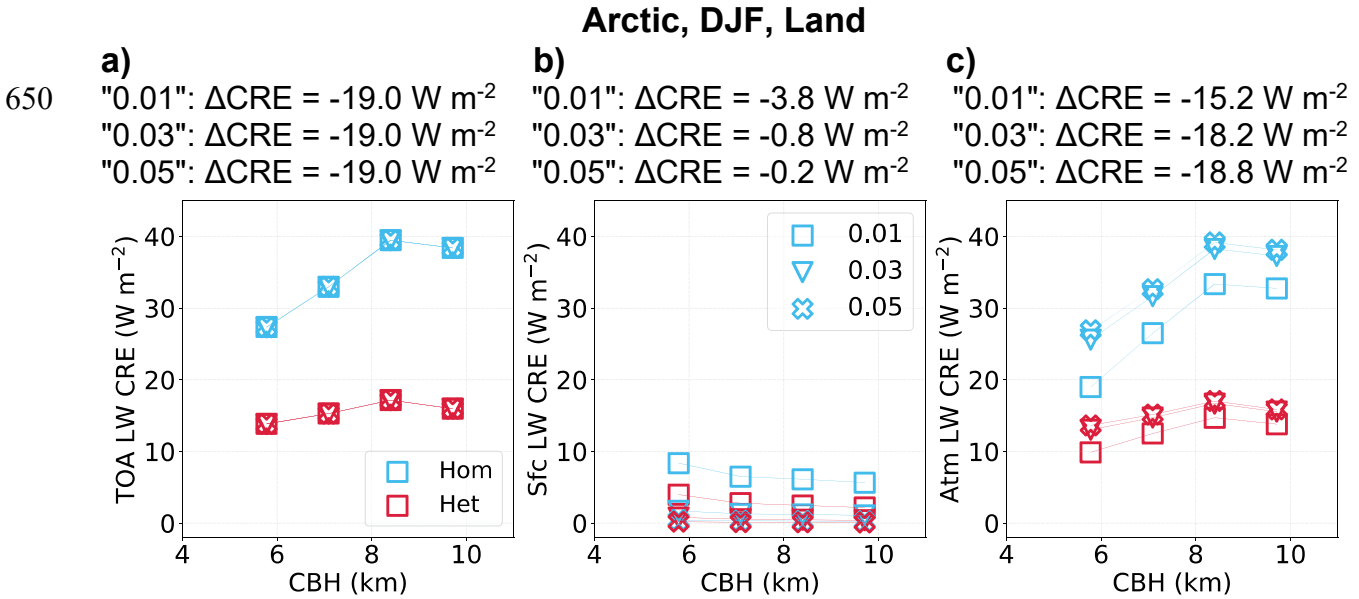


Figure 10. Sensitivity of RTM-simulated cirrus CRE to three different low liquid clouds with varying liquid water content (LWC) values of 0.01, 0.03, and 0.05  $\text{g m}^{-3}$ .

At the surface, however, cirrus LW CRE decreases rapidly as low cloud LWC increases. Note that the largest LWC selected here ( $0.05 \text{ g m}^{-3}$ ) is at the lower end of typical LWC values observed in the Arctic (Achttert et al., 2020). Our results demonstrate that low liquid clouds  $\sim 600 \text{ m}$  thick with a LWC greater than  $0.05 \text{ g m}^{-3}$  act more like a “black body”, absorbing/emitting almost all the downward LW radiation emitted by cirrus clouds.

The presence of low clouds has little effect on the transition from homogeneous to heterogeneous cirrus at the TOA, with  $\Delta\text{CRE}$  remaining at  $-19.0 \text{ W m}^{-2}$ . However, it considerably reduces  $\Delta\text{CRE}$  at the surface, from  $-3.8 \text{ W m}^{-2}$  (for LWC =  $0.01 \text{ g m}^{-3}$ ) to  $-0.2 \text{ W m}^{-2}$  (for LWC =  $0.05 \text{ g m}^{-3}$ ). As a result, the atmospheric  $\Delta\text{CRE}$  remains between  $-15.2 \text{ W m}^{-2}$  and  $-18.8 \text{ W m}^{-2}$ . These results imply that while the instantaneous efficacy of CCT is negligible in the presence of low liquid clouds, its potential efficacy could still influence the surface through feedback processes over longer timescales.

### 4.3 Sensitivity to Arctic aerosols

In the past, the Arctic atmosphere was considered pristine, but over the past decades, it has been revealed that Arctic aerosols play an important role through aerosol-radiation interactions (Thorsen and Fu, 2015) and aerosol-cloud interactions (Creamean et al., 2021; Zamora et al., 2016). Both observations (Dagsson-Waldhauserova et al., 2019) and numerical simulations (Breider et al., 2014) showed that Arctic aerosol concentrations vary with season with the main peak in late winter and spring, and another peak in fall. The major peak is known as the Arctic haze, a phenomenon mainly caused by the transport of industrial anthropogenic aerosols from Europe and Asia that remain in the Arctic atmosphere due to a stable atmosphere and a lack of precipitation (Schmale et al., 2022). With the reduction of anthropogenic aerosols in summer, natural aerosols, including sea spray and organic compounds, dominate (Moschos et al., 2022). Another important aerosol type in the Arctic is dust with its maximum in late winter and early spring due to the long-range transport from Asia and Africa and its minimum in summer and fall predominantly because of local sources (Groot Zwaaftink et al., 2016; Xie et al., 2022).

Our RTM simulations evaluate the sensitivity of cirrus CRE to different aerosol scenarios, as explained in Sect. 2. The results (Fig. S4) show that aerosol type and concentration have a

685 relatively small impact on cirrus LW CRE. This finding is consistent with previous studies, which  
have demonstrated that while aerosols absorb SW radiation, they are weak absorbers of LW  
radiation (Bergstrom et al., 2007; Samset et al., 2018). As a result, the cooling effect of  
transitioning from homogeneous to heterogeneous cirrus is not sensitive to the choice of aerosol  
scenarios, with TOA  $\Delta$ CRE ranging from -19.3 to -19.8  $\text{W m}^{-2}$ , Sfc  $\Delta$ CRE from -10.2 to -10.4  $\text{W}$   
690  $\text{m}^{-2}$ , and Atm  $\Delta$ CRE from -9.1 to -9.4  $\text{W m}^{-2}$ . It is important to note that the modeling design here  
only accounts for the aerosol direct effect, as the RTM cannot simulate aerosol indirect effects.  
However, it would be possible to study such effect if cloud profiles are carefully explored and  
grouped based on aerosol loading.

695 **5 Suggestions for improving cirrus cloud modeling**

In previous sections, we implemented retrieved cloud microphysical products from satellite in an  
RTM to estimate the instantaneous cirrus CRE. RTMs have fewer degrees of freedom than GCMs,  
and this makes them more convenient for interpreting changes in cirrus radiative impacts.  
However, GCMs are the ultimate tool for determining the global cirrus CRE since they account  
700 for climate feedback processes which are expected to enhance the CRE predicted by an RTM. That  
is, the direct CCT polar cooling predicted by an RTM may promote coverage by snow and sea ice  
(Storelvmo et al., 2014), enhancing planetary albedo and thus cooling. Despite their advantages,  
GCMs face several challenges in accurately representing cirrus clouds. Below, we briefly discuss  
these issues and propose improvements based on recent research.

705 GCMs employ ice parameterizations that are often based on limited observations and therefore,  
uncertainties could arise when generalizing those formulations (Eidhammer et al., 2017; Gettelman  
and Morrison, 2015). In particular, many field campaigns do not sample homogeneous cirrus  
clouds sufficiently. Also, in prognostic modeling frameworks, the competition between  
heterogeneous and homogeneous ice nucleation remains a complex process (Barahona and Nenes,  
710 Kärcher et al., 2022; Spichtinger and Cziczo, 2010; Spichtinger and Gierens, 2009). Current  
GCMs might underestimate the contribution of homogeneous nucleation, particularly outside the  
tropics during the winter season, when INP concentrations appear to be lower (Carlsen and David,

2022; Mitchell and Garnier, 2024). For example, the GCM simulations of Gasparini and Lohmann (2016) predict homogeneous nucleation dominating only below  $\sim 250$  hPa ( $< \sim 11$  km) when pre-existing ice was not considered, and the main CCT simulations in Tully et al. (2022, 2023) did not consider orographic gravity wave (OGW) induced cirrus clouds. This differs from the CALIPSO-derived results in Mitchell and Garnier (2024, Fig. 19) that show homogeneous cirrus clouds contributing significantly at all cirrus levels, with evidence that a substantial percentage of these homogeneous cirrus clouds are OGW cirrus clouds. This shortcoming in GCMs can lead to an underestimation of the radiative effects of cirrus clouds and the potential cooling efficacy of CCT. To address this, GCMs could use satellite retrievals of  $N_i$ ,  $D_e$ , and IWC when developing/constraining parameterizations that represent the two cirrus regimes.

On the other hand, the GCM-CCT modeling study by Gasparini and Lohmann (2016) found that INP seeding affects mostly in situ cirrus clouds, with only minor impacts on cirrus clouds resulting from strong dynamical forcing, such as OGW cirrus clouds. While this has not been confirmed by observations (e.g., from a field experiment), it appears plausible that INP seeding may not sufficiently reduce the RH<sub>i</sub> in the stronger OGW cirrus updrafts to prevent homogeneous freezing. This factor may introduce a positive bias in the CCT cooling estimates from this study.

A critical factor in modeling cirrus clouds is the treatment of pre-existing ice, which refers to ice particles already present before the formation of new ice particles. This treatment enhances the contribution of heterogeneous nucleation. Therefore, including pre-existing ice in GCMs significantly reduces  $N_i$ , as shown in simulations comparing models with and without pre-existing ice (Shi et al., 2015). As explained by Mitchell and Erfani (2025) and Mitchell and Garnier (2024), the current treatment of the pre-existing ice in GCMs leads to an overestimation of pre-existing ice effect, which can bias the homogeneous and heterogeneous contributions and their radiative effects. Using models with higher vertical resolution, such as RCMs or large-eddy simulations (LES), can help mitigate the overestimation of pre-existing ice by better resolving vertical gradients of mixing ratio, temperature, and vertical velocity, which are critical for accurately capturing ice nucleation processes.

Another important factor in cirrus cloud modeling is the role of OGWS. OGWS are expected to promote homogeneous ice nucleation in cirrus clouds by increasing their updrafts and

supersaturations. Recent studies have demonstrated that including OGWs in GCMs leads to stronger homogeneous ice nucleation, and thereby higher  $N_i$  and IWC and lower  $D_e$  (Lyu et al., 2023; Tully et al., 2022), highlighting the importance of OGWs in GCMs.

745 Furthermore, GCMs should account for complex processes for underlying mixed-phase clouds and their relationship with cirrus clouds. Through injecting INPs, CCT can modify cirrus cloud microphysics (e.g. reductions in  $N_i$  and increases in  $D_e$ ) which then affects the growth processes of ice particles in mixed-phase clouds that causes additional cooling (Gruber et al., 2019; Mitchell et al., 2020). This realization helped give birth to a new climate intervention method known as  
750 mixed-phase regime cloud thinning or MCT (Villanueva et al., 2022). In the CCT investigation described in Mitchell et al. (2020), most of the CCT CRE was due to mixed phase clouds that were affected by microphysical changes in the overlying cirrus clouds. This suggests that the glaciation of mixed phase clouds with subsequent CRE changes may be partly accomplished through CCT using INP concentrations on the order of  $10 \text{ L}^{-1}$  (Storelvmo et al., 2013; 2014) instead of the higher  
755 INP concentrations indicated in Villanueva et al. (2022), which were on the order of  $10^5 \text{ L}^{-1}$  in the Arctic for producing a CRE change of  $-1 \text{ W m}^{-2}$ . This approach may also produce a CRE change or cooling effect greater than the CRE change produced by CCT or MCT alone.

Another significant gap in CCT research is the lack of process-based modeling using high vertical and/or horizontal resolutions such as LES and single column models. To the best of our knowledge, 760 only one LES study has been conducted on CCT (Gruber et al., 2019). This limits our understanding of smaller-scale processes such as turbulence (Kärcher et al., 2025), convection, and cloud physics in cirrus clouds. In contrast, extensive LES research has been employed for another SRM method, called marine cloud brightening (MCB), in order to resolve those processes (Chun et al., 2023; Erfani et al., 2022, 2024). The knowledge gained from such studies can then  
765 be employed to improve the representation of MCB in GCMs. Similar efforts are needed for understanding processes related to CCT. In particular, two of the aforementioned issues, pre-existing ice treatment and OGW parameterization, should not be significant in high-resolution LES experiments.

770 **6 Conclusions**

This study investigates CCT as a climate intervention method by quantifying it as the transition from homogeneous to heterogeneous cirrus clouds. Considering the challenges of achieving rapid GHG emission reductions, it has been argued that climate intervention methods may be necessary to mitigate global warming (Baiman et al., 2024; Kriegler et al., 2018). However, modifying the environment involves many risks, including unintended consequences for air quality, weather, and climate (Blackstock et al., 2009; Pereira et al., 2021). For this reason, it is important to conduct comprehensive research in order to quantify the efficacy, risks, costs, and limitations of such methods. Even if these methods pass all necessary tests, they are not alternatives to GHG emission reduction; rather, they are intended to "buy time" for societies to avoid the worst consequences of climate change until GHG emissions (and concentrations perhaps) are reduced to safe levels.

GCMs are advantageous for identifying the global net forcing of cirrus clouds, while accounting for climate feedback processes. However, inaccurate cirrus cloud processes (e.g., INP concentrations and vertical motions at cirrus cloud levels) and resolution-dependent parameterizations (e.g., pre-existing ice treatment) cause uncertainties in GCM simulations of CCT. For instance, GCMs that did not account for pre-existing ice predicted efficient CCT cooling (Storelvmo et al., 2013, 2014; Gasparini et al., 2020), while those that implemented pre-existing ice suggested minimal or adverse CCT effects (Gasparini and Lohmann, 2016; Tully et al., 2022, 2023). In contrast, process-based models, such as the RTM used in this study, may more easily be constrained with satellite measurements of cirrus cloud properties and help isolate certain mechanisms. That knowledge can then be used to improve GCMs.

This study integrates the CALIPSO satellite retrievals described in Mitchell and Garnier (2024) with the libRadtran RTM to improve estimates of the radiative effects of homogeneous and heterogeneous cirrus clouds. Our results confirm that homogeneous cirrus clouds exert a significantly stronger CRE than heterogeneous cirrus, which implies that transitioning from homogeneous to heterogeneous cirrus, as a means of quantifying the first CCT scenario, can result in substantial cooling in polar regions during winter. Our estimated surface cooling in the Polar Regions (which we call instantaneous CCT efficacy) ranges from  $-0.7$  to  $-1.0 \text{ W m}^{-2}$ , with a TOA cooling of  $-1.2$  to  $-1.6 \text{ W m}^{-2}$ . However, the second CCT scenario, the impact of "new cirrus"

formation from injected INPs in clear-sky ice-supersaturated regions opposes the first scenario. As  
800 a result, the estimated total surface cooling effects range from  $-0.2$  to  $-0.5 \text{ W m}^{-2}$  and the total TOA  
cooling ranges from  $-0.3$  to  $-0.9 \text{ W m}^{-2}$ . These values fall within the cooling range of  $-0.25$  to  $-2$   
 $\text{W m}^{-2}$  estimated by previous GCM studies (Gasparini et al., 2020; Gasparini and Lohmann, 2016;  
Storelvmo et al., 2013; Storelvmo and Herger, 2014; Storelvmo et al., 2014).

A major concern raised by previous CCT studies is *overseeding*, where injecting excessive INPs  
805 forms too many small ice particles through heterogeneous nucleation in cirrus clouds, leading to  
higher optical thickness, longer cloud lifetime, and ultimately a warming effect (Gasparini and  
Lohmann, 2016; Penner et al., 2015; Storelvmo et al., 2013; Tully et al., 2022). A related seeding  
concern is the creation of new cirrus clouds in clear sky regions where the  $\text{RH}_i$  is above ice  
saturation and natural INP concentrations are relatively low. By nature, RTMs cannot directly test  
810 these side effects or any other adjustment or feedback process. However, regarding the latter,  
Gruber et al. (2019) investigated CCT for an Arctic case study using the ICON-ART modeling  
system with a horizontal resolution of 5 km and an integration time step of 25 s, and found that  
while seeding produced some new cirrus clouds, these new cirrus suppressed homogeneous  
nucleation downstream by lowering  $\text{RH}_i$  further downstream, with these two phenomena tending  
815 to cancel in terms of their radiative effect. And in regard to overseeding, this rarely occurred since  
homogeneous nucleation in natural cirrus was active throughout most of the model domain.  
Another concern is the potential impact of CCT on precipitation; however, this impact seems to  
be small as a change in cirrus CRE caused by CCT can lead to a global mean rainfall reduction of  
-1.3%, which is less than corresponding estimates for another climate engineering SRM method  
820 known as stratospheric aerosol injection (Storelvmo et al., 2014).

Over the mid-latitudes during winter, RTM simulations show slight CCT warming at the TOA and  
within the atmosphere and no significant impact at the surface due to competing LW and SW  
radiation effects: homogeneous cirrus absorbs/emits more LW radiation but also scatters more SW  
radiation than heterogeneous cirrus and these two effects cancel each other at the surface. This  
825 finding is consistent with Storelvmo et al. (2014), who suggested that conducting CCT globally is  
not more efficient than targeting high-latitude regions.

Sensitivity analyses reveal that the cooling efficacy of CCT is significantly affected by atmospheric thermodynamic profiles and the presence of low clouds. TOA cooling is sensitive to surface temperature, while surface cooling is less sensitive to changes in atmospheric water vapor.

830 These findings align with previous studies (Corti and Peter, 2009; Dupont and Haeffelin, 2008), which demonstrated that cirrus CRE at the TOA depends on the temperature contrast between the Earth's surface and the cloud, whereas the cirrus CRE at the surface is reduced by a more humid atmosphere due to the absorption of downward LW radiation by water vapor. Furthermore, these results indicate that Arctic low clouds tend to strongly suppress the instantaneous efficacy of CCT

835 by insulating the surface from the CCT atmospheric cooling. However, this strong atmospheric cooling suggests that CCT may still influence the surface through mixing and other feedback mechanisms over longer timescales, even in the presence of low clouds. In addition, some studies indicated that winter-time Arctic low cloud cover has decreased in recent decades (Boccolari and Parmiggiani, 2018; Liu and Key, 2016; Schweiger, 2004; Wang and Key, 2003), which implies

840 stronger potential for instantaneous impact of CCT at the surface in the future.

Our study highlights the necessity of improving the representation of cirrus cloud processes in models, particularly the radiative contributions of the homogeneous and heterogeneous regimes. To more accurately quantify the efficacy of CCT, future work should focus on 1) using satellite retrievals of cirrus cloud properties to guide corresponding model parameterizations, 2) revisiting

845 assumptions such as the treatment of pre-existing ice in GCMs, 3) including OGW cirrus clouds in GCMs, and 4) employing high-resolution LES experiments. While LES modeling has been widely used in studies of another climate intervention method (i.e., MCB) to resolve smaller-scale processes (Chun et al., 2023; Erfani et al., 2022, 2024), its application to CCT remains limited to a single study (e.g., Gruber et al., 2019). Considering the persistent uncertainties in observing and

850 modeling aerosol-cloud-precipitation interactions related to cirrus clouds, an integration of spatially and temporally high-resolution in-situ and/or remote sensing measurements may be essential for constraining parameterizations and for improving the representation of ice processes in LES and GCM modeling. In the future, we will incorporate CALIPSO retrievals of cirrus clouds into the NCAR GCM known as the Community Atmosphere Model, version 6 (CAM6) to quantify

855  $D_e$  as a function of IWC and  $T$  for heterogeneous freezing only and for observed cirrus cloud

conditions (where both heterogeneous and homogeneous freezing are active), based on the same CALIPSO retrievals used here. This analysis will be region- and season-dependent.

**860 Data Availability Statement:** The MERRA2 reanalysis data is publicly available at <https://doi.org/10.5067/2E096JV59PK7> (Global Modeling and Assimilation Office (GMAO), 2015). The libRadtran code is publicly accessible at <http://www.libradtran.org/doku.php> (Emde et al., 2016). The CALIPSO retrievals of IWC and  $D_e$  from Mitchell and Garnier (2024), and the RTM outputs in this study will be provided upon request.

**865 Competing interests:** The authors declare that no competing interests are present.

**870 Author contributions:** All co-authors contributed to the conceptualization, methodology, and discussions about interpreting the results. EE developed the Python codes and conducted exploratory data analysis and RTM simulations. EE drafted the manuscript, and all co-authors provided edits and revisions.

**875 Acknowledgments:** This study was primarily supported by NOAA's Climate Program Office Earth's Radiation Budget (ERB) Program, Grant NA22OAR4690640. We appreciate two anonymous reviewers for their constructive comments and Anne Garnier, Marco Giordano, John Mejia, Blaž Gasparini, and Claudia Emde for discussions on this research that contributed to the improvement of the final results.

## References

**880 Achtert, P., O'Connor, E. J., Brooks, I. M., Sotiropoulou, G., Shupe, M. D., Pospichal, B., Brooks, B. J., and Tjernström, M.: Properties of Arctic liquid and mixed-phase clouds from**

shipborne Cloudnet observations during ACSE 2014, *Atmospheric Chemistry and Physics*, 20, 14983–15002, <https://doi.org/10.5194/acp-20-14983-2020>, 2020.

885 Aktaş, A. and Kirçiçek, Y.: Chapter 13 - Examples of Solar Hybrid System Layouts, Design Guidelines, Energy Performance, Economic Concern, and Life Cycle Analyses, in: *Solar Hybrid Systems*, edited by: Aktaş, A. and Kirçiçek, Y., Academic Press, 331–349, <https://doi.org/10.1016/B978-0-323-88499-0.00013-6>, 2021.

Anderson, G. P., Clough, S. A., Kneizys, F., Chetwynd, J. H., and Shettle, E. P.: AFGL atmospheric constituent profiles (0.120 km), Air Force Geophysics Lab Hanscom AFB MA, 1986.

890 Baiman, R., Clarke, S., Elsworth, C., Field, L., MacCracken, M., Macdonald, J., Mitchell, D., Oeste, F. D., Reed, S., Salter, S., Simmens, H., Tao, Y., and Tulip, R.: Addressing the urgent need for direct climate cooling: Rationale and options, *Oxford Open Climate Change*, 4, kgae014, <https://doi.org/10.1093/oxfclm/kgae014>, 2024.

895 Barahona, D. and Nenes, A.: Parameterizing the competition between homogeneous and heterogeneous freezing in ice cloud formation – polydisperse ice nuclei, *Atmospheric Chemistry and Physics*, 9, 5933–5948, <https://doi.org/10.5194/acp-9-5933-2009>, 2009.

Baum, B. A., Yang, P., Heymsfield, A. J., Platnick, S., King, M. D., Hu, Y.-X., and Bedka, S. T.: Bulk Scattering Properties for the Remote Sensing of Ice Clouds. Part II: Narrowband Models, *Journal of Applied Meteorology*, 44, 1896–1911, <https://doi.org/10.1175/JAM2309.1>, 2005.

900 Bergstrom, R. W., Pilewskie, P., Russell, P. B., Redemann, J., Bond, T. C., Quinn, P. K., and Sierau, B.: Spectral absorption properties of atmospheric aerosols, *Atmospheric Chemistry and Physics*, 7, 5937–5943, <https://doi.org/10.5194/acp-7-5937-2007>, 2007.

905 Boccolari, M. and Parmiggiani, F.: Trends and variability of cloud fraction cover in the Arctic, 1982–2009, *Theor Appl Climatol*, 132, 739–749, <https://doi.org/10.1007/s00704-017-2125-6>, 2018.

Breider, T. J., Mickley, L. J., Jacob, D. J., Wang, Q., Fisher, J. A., Chang, Rachel. Y.-W., and Alexander, B.: Annual distributions and sources of Arctic aerosol components, aerosol optical depth, and aerosol absorption: Ann. dist. & sources of Arctic aerosol, *J. Geophys. Res. Atmos.*, 119, 4107–4124, <https://doi.org/10.1002/2013JD020996>, 2014.

910 Buras, R., Dowling, T., and Emde, C.: New secondary-scattering correction in DISORT with increased efficiency for forward scattering, *Journal of Quantitative Spectroscopy and Radiative Transfer*, 112, 2028–2034, <https://doi.org/10.1016/j.jqsrt.2011.03.019>, 2011.

915 Carlsen, T. and David, R. O.: Spaceborne Evidence That Ice-Nucleating Particles Influence High-Latitude Cloud Phase, *Geophysical Research Letters*, 49, e2022GL098041, <https://doi.org/10.1029/2022GL098041>, 2022.

Chun, J.-Y., Wood, R., Blossey, P., and Doherty, S. J.: Microphysical, macrophysical, and radiative responses of subtropical marine clouds to aerosol injections, *Atmospheric Chemistry and Physics*, 23, 1345–1368, <https://doi.org/10.5194/acp-23-1345-2023>, 2023.

920 Cirisan, A., Spichtinger, P., Luo, B. P., Weisenstein, D. K., Wernli, H., Lohmann, U., and Peter, T.: Microphysical and radiative changes in cirrus clouds by geoengineering the stratosphere, *Journal of Geophysical Research: Atmospheres*, 118, 4533–4548, <https://doi.org/10.1002/jgrd.50388>, 2013.

925 Cohen, J., Zhang, X., Francis, J., Jung, T., Kwok, R., Overland, J., Ballinger, T. J., Bhatt, U. S., Chen, H. W., Coumou, D., Feldstein, S., Gu, H., Handorf, D., Henderson, G., Ionita, M., Kretschmer, M., Laliberte, F., Lee, S., Linderholm, H. W., Maslowski, W., Peings, Y., Pfeiffer, K., Rigor, I., Semmler, T., Stroeve, J., Taylor, P. C., Vavrus, S., Vihma, T., Wang, S., Wendisch, M., Wu, Y., and Yoon, J.: Divergent consensuses on Arctic amplification influence on midlatitude severe winter weather, *Nat. Clim. Chang.*, 10, 20–29, <https://doi.org/10.1038/s41558-019-0662-y>, 2020.

930 Córdoba-Jabonero, C., Gómez-Martín, L., del Águila, A., Vilaplana, J. M., López-Cayuela, M.-Á., and Zorzano, M.-P.: Cirrus-induced shortwave radiative effects depending on their optical and physical properties: Case studies using simulations and measurements, *Atmospheric Research*, 246, 105095, <https://doi.org/10.1016/j.atmosres.2020.105095>, 2020.

935 Corti, T. and Peter, T.: A simple model for cloud radiative forcing, *Atmospheric Chemistry and Physics*, 9, 5751–5758, <https://doi.org/10.5194/acp-9-5751-2009>, 2009.

Creamean, J. M., de Boer, G., Telg, H., Mei, F., Dexheimer, D., Shupe, M. D., Solomon, A., and McComiskey, A.: Assessing the vertical structure of Arctic aerosols using balloon-borne measurements, *Atmospheric Chemistry and Physics*, 21, 1737–1757, <https://doi.org/10.5194/acp-21-1737-2021>, 2021.

940 Cziczo, D. J., Froyd, K. D., Hoose, C., Jensen, E. J., Diao, M., Zondlo, M. A., Smith, J. B., Twohy, C. H., and Murphy, D. M.: Clarifying the Dominant Sources and Mechanisms of Cirrus Cloud Formation, *Science*, 340, 1320–1324, <https://doi.org/10.1126/science.1234145>, 2013.

945 Dagsson-Waldhauserova, P., Renard, J.-B., Olafsson, H., Vignelles, D., Berthet, G., Verdier, N., and Duverger, V.: Vertical distribution of aerosols in dust storms during the Arctic winter, *Sci Rep*, 9, 16122, <https://doi.org/10.1038/s41598-019-51764-y>, 2019.

Dowling, D. R. and Radke, L. F.: A Summary of the Physical Properties of Cirrus Clouds, *Journal of Applied Meteorology and Climatology*, 29, 970–978, [https://doi.org/10.1175/1520-0450\(1990\)029<0970:ASOTPP>2.0.CO;2](https://doi.org/10.1175/1520-0450(1990)029<0970:ASOTPP>2.0.CO;2), 1990.

950 Dupont, J.-C. and Haeffelin, M.: Observed instantaneous cirrus radiative effect on surface-level shortwave and longwave irradiances, *Journal of Geophysical Research: Atmospheres*, 113, <https://doi.org/10.1029/2008JD009838>, 2008.

Eastman, R. and Warren, S. G.: Interannual Variations of Arctic Cloud Types in Relation to Sea Ice, *Journal of Climate*, 23, 4216–4232, <https://doi.org/10.1175/2010JCLI3492.1>, 2010.

955 Eidhammer, T., Morrison, H., Mitchell, D., Gettelman, A., and Erfani, E.: Improvements in Global Climate Model Microphysics Using a Consistent Representation of Ice Particle Properties, <https://doi.org/10.1175/JCLI-D-16-0050.1>, 2017.

Eliasson, S., Buehler, S. A., Milz, M., Eriksson, P., and John, V. O.: Assessing observed and modelled spatial distributions of ice water path using satellite data, *Atmospheric Chemistry and Physics*, 11, 375–391, <https://doi.org/10.5194/acp-11-375-2011>, 2011.

960 Emde, C., Buras-Schnell, R., Kylling, A., Mayer, B., Gasteiger, J., Hamann, U., Kylling, J., Richter, B., Pause, C., Dowling, T., and Bugliaro, L.: The libRadtran software package for radiative transfer calculations (version 2.0.1), *Geosci. Model Dev.*, 9, 1647–1672, <https://doi.org/10.5194/gmd-9-1647-2016>, 2016.

965 Erfani, E. and Mitchell, D. L.: Developing and bounding ice particle mass- and area-dimension expressions for use in atmospheric models and remote sensing, *Atmos. Chem. Phys.*, 16, 4379–4400, <https://doi.org/10.5194/acp-16-4379-2016>, 2016.

Erfani, E. and Mitchell, D. L.: Growth of ice particle mass and projected area during riming, *Atmospheric Chemistry and Physics*, 17, 1241–1257, <https://doi.org/10.5194/acp-17-1241-2017>, 2017.

970 Erfani, E., Blossey, P., Wood, R., Mohrmann, J., Doherty, S. J., Wyant, M., and O, K.: Simulating Aerosol Lifecycle Impacts on the Subtropical Stratocumulus-to-Cumulus Transition Using Large-Eddy Simulations, *Journal of Geophysical Research: Atmospheres*, 127, e2022JD037258, <https://doi.org/10.1029/2022JD037258>, 2022.

975 Erfani, E., Wood, R., Blossey, P., Doherty, S. J., and Eastman, R.: Building a comprehensive library of observed Lagrangian trajectories for testing modeled cloud evolution, aerosol-cloud interactions, and marine cloud brightening, *EGUphere*, 1–52, <https://doi.org/10.5194/egusphere-2024-3232>, 2024.

980 Evans, K. F., Wang, J. R., O’C Starr, D., Heymsfield, G., Li, L., Tian, L., Lawson, R. P., Heymsfield, A. J., and Bansemer, A.: Ice hydrometeor profile retrieval algorithm for high-frequency microwave radiometers: application to the CoSSIR instrument during TC4, *Atmos. Meas. Tech.*, 5, 2277–2306, <https://doi.org/10.5194/amt-5-2277-2012>, 2012.

985 Fauchez, T., Davis, A. B., Cornet, C., Szczap, F., Platnick, S., Dubuisson, P., and Thieuleux, F.: A fast hybrid (3-D/1-D) model for thermal radiative transfer in cirrus via successive orders of scattering, *Journal of Geophysical Research: Atmospheres*, 122, 344–366, <https://doi.org/10.1002/2016JD025607>, 2017.

Forster, P., Storelvmo, T., Armour, K., Collins, W., Dufresne, J.-L., Frame, D., Lunt, D., Mauritzen, T., Palmer, M., and Watanabe, M.: The Earth’s energy budget, climate feedbacks, and climate sensitivity, in: *Climate Change 2021: The Physical Science Basis. Contribution of*

990 Working Group I to the Sixth Assessment Report of the Intergovernmental Panel on Climate Change [Masson-Delmotte, V., P. Zhai, A. Pirani, S. L. Connors, C. Péan, S. Berger, N. Caud, Y. Chen, L. Goldfarb, M. I. Gomis, M. Huang, K. Leitzell, E. Lonnoy, J.B.R. Matthews, T. K. Maycock, T. Waterfield, O. Yelekçi, R. Yu and B. Zhou (eds.)], Cambridge University Press, Cambridge, United Kingdom, 2021.

995 Froyd, K. D., Yu, P., Schill, G. P., Brock, C. A., Kupc, A., Williamson, C. J., Jensen, E. J., Ray, E., Rosenlof, K. H., Bian, H., Darmenov, A. S., Colarco, P. R., Diskin, G. S., Bui, T., and Murphy, D. M.: Dominant role of mineral dust in cirrus cloud formation revealed by global-scale measurements, *Nat. Geosci.*, 15, 177–183, <https://doi.org/10.1038/s41561-022-00901-w>, 2022.

1000 Fu, Q. and Liou, K. N.: Parameterization of the Radiative Properties of Cirrus Clouds, *Journal of the Atmospheric Sciences*, 50, 2008–2025, [https://doi.org/10.1175/1520-0469\(1993\)050<2008:POTRPO>2.0.CO;2](https://doi.org/10.1175/1520-0469(1993)050<2008:POTRPO>2.0.CO;2), 1993.

Gao, B.-C., Yang, P., Han, W., Li, R.-R., and Wiscombe, W. J.: An algorithm using visible and 1.38-spl mu/m channels to retrieve cirrus cloud reflectances from aircraft and satellite data, *IEEE Transactions on Geoscience and Remote Sensing*, 40, 1659–1668, 2002.

1005 Gasparini, B. and Lohmann, U.: Why cirrus cloud seeding cannot substantially cool the planet, *J. Geophys. Res. Atmos.*, 121, 4877–4893, <https://doi.org/10.1002/2015JD024666>, 2016.

Gasparini, B., McGraw, Z., Storelvmo, T., and Lohmann, U.: To what extent can cirrus cloud seeding counteract global warming?, *Environ. Res. Lett.*, 15, 054002, <https://doi.org/10.1088/1748-9326/ab71a3>, 2020.

1010 Gasparini, B., Sullivan, S. C., Sokol, A. B., Kärcher, B., Jensen, E., and Hartmann, D. L.: Opinion: Tropical cirrus – from micro-scale processes to climate-scale impacts, *Atmospheric Chemistry and Physics*, 23, 15413–15444, <https://doi.org/10.5194/acp-23-15413-2023>, 2023.

1015 Gasteiger, J., Emde, C., Mayer, B., Buras, R., Buehler, S. A., and Lemke, O.: Representative wavelengths absorption parameterization applied to satellite channels and spectral bands, *Journal of Quantitative Spectroscopy and Radiative Transfer*, 148, 99–115, <https://doi.org/10.1016/j.jqsrt.2014.06.024>, 2014.

Gelaro, R., McCarty, W., Suárez, M. J., Todling, R., Molod, A., and Takacs, L.: The modern-era retrospective analysis for research and applications, version 2 (MERRA-2), *J. Clim.*, 30, 5419–5454, <https://doi.org/10.1175/JCLI-D-16-0758.1>, 2017.

1020 Gettelman, A. and Morrison, H.: Advanced Two-Moment Bulk Microphysics for Global Models. Part I: Off-Line Tests and Comparison with Other Schemes, *J. Clim.*, 28, 1268–1287, <https://doi.org/10.1175/jcli-d-14-00102.1>, 2015.

1025 Global Modeling and Assimilation Office (GMAO): MERRA-2 inst3\_3d\_asm\_Np: 3d,3-Hourly,Instantaneous,Pressure-Level,Assimilation,Assimilated Meteorological Fields V5.12.4, Greenbelt, MD, USA, Goddard Earth Sciences Data and Information Services Center (GES DISC)[Dataset], <https://doi.org/10.5067/QBZ6MG944HW0>, 2015c.

Gouveia, D. A., Barja, B., Barbosa, H. M. J., Seifert, P., Baars, H., Pauliquevis, T., and Artaxo, P.: Optical and geometrical properties of cirrus clouds in Amazonia derived from 1 year of ground-based lidar measurements, *Atmospheric Chemistry and Physics*, 17, 3619–3636, <https://doi.org/10.5194/acp-17-3619-2017>, 2017.

1030 Groot Zwaaftink, C. D., Grythe, H., Skov, H., and Stohl, A.: Substantial contribution of northern high-latitude sources to mineral dust in the Arctic, *Journal of Geophysical Research: Atmospheres*, 121, 13,678-13,697, <https://doi.org/10.1002/2016JD025482>, 2016.

1035 Gruber, S., Blahak, U., Haenel, F., Kottmeier, C., Leisner, T., Muskatel, H., Storelvmo, T., and Vogel, B.: A Process Study on Thinning of Arctic Winter Cirrus Clouds With High-Resolution ICON-ART Simulations, *Journal of Geophysical Research: Atmospheres*, 124, 5860–5888, <https://doi.org/10.1029/2018JD029815>, 2019.

1040 Gryspeerdt, E., Sourdeval, O., Quaas, J., Delanoë, J., Krämer, M., and Kühne, P.: Ice crystal number concentration estimates from lidar–radar satellite remote sensing – Part 2: Controls on the ice crystal number concentration, *Atmospheric Chemistry and Physics*, 18, 14351–14370, <https://doi.org/10.5194/acp-18-14351-2018>, 2018.

1045 Guignard, A., Stubenrauch, C. J., Baran, A. J., and Armante, R.: Bulk microphysical properties of semi-transparent cirrus from AIRS: a six year global climatology and statistical analysis in synergy with geometrical profiling data from CloudSat-CALIPSO, *Atmos. Chem. Phys.*, 12, 503–525, <https://doi.org/10.5194/acp-12-503-2012>, 2012.

Hartmann, D. L.: Global physical climatology, 2nd ed., Elsevier Science, Amsterdam, 485 pp., 2016.

1050 Heymsfield, A. J., Krämer, M., Luebke, A., Brown, P., Cziczo, D. J., Franklin, C., Lawson, P., Lohmann, U., McFarquhar, G., Ulanowski, Z., and Tricht, K. V.: Cirrus Clouds, Meteorological Monographs, 58, 2.1-2.26, <https://doi.org/10.1175/AMSMONOGRAPH-D-16-0010.1>, 2017.

1055 Hong, Y., Liu, G., and Li, J.-L. F.: Assessing the Radiative Effects of Global Ice Clouds Based on CloudSat and CALIPSO Measurements, *Journal of Climate*, 29, 7651–7674, <https://doi.org/10.1175/JCLI-D-15-0799.1>, 2016.

Hu, Y. X. and Stamnes, K.: An Accurate Parameterization of the Radiative Properties of Water Clouds Suitable for Use in Climate Models, *Journal of Climate*, 6, 728–742, [https://doi.org/10.1175/1520-0442\(1993\)006<0728:AAPOTR>2.0.CO;2](https://doi.org/10.1175/1520-0442(1993)006<0728:AAPOTR>2.0.CO;2), 1993.

1060 Huang, Y., Dong, X., Kay, J. E., Xi, B., and McIlhattan, E. A.: The climate response to increased cloud liquid water over the Arctic in CESM1: a sensitivity study of Wegener–Bergeron–Findeisen process, *Clim Dyn*, 56, 3373–3394, <https://doi.org/10.1007/s00382-021-05648-5>, 2021.

IPCC report: Technical summary, in: Climate Change 2021: The Physical Science Basis. Contribution of Working Group I to the Sixth Assessment Report of the Intergovernmental Panel

on Climate Change, Cambridge University Press, Cambridge, United Kingdom and New York, NY, USA, 33–144, <https://doi.org/10.1017/9781009157896.001>, 2021.

1065 Järvinen, E., Nehlert, F., Xu, G., Waitz, F., Mioche, G., Dupuy, R., Jourdan, O., and Schnaiter, M.: Investigating the vertical extent and short-wave radiative effects of the ice phase in Arctic summertime low-level clouds, *Atmospheric Chemistry and Physics*, 23, 7611–7633, <https://doi.org/10.5194/acp-23-7611-2023>, 2023.

1070 Jiang, J. H., Yue, Q., Su, H., Kangaslahti, P., Lebsack, M., Reising, S., Schoeberl, M., Wu, L., and Herman, R. L.: Simulation of Remote Sensing of Clouds and Humidity From Space Using a Combined Platform of Radar and Multifrequency Microwave Radiometers, *Earth and Space Science*, 6, 1234–1243, <https://doi.org/10.1029/2019EA000580>, 2019.

1075 Kanji, Z. A., Ladino, L. A., Wex, H., Boose, Y., Burkert-Kohn, M., Cziczo, D. J., and Krämer, M.: Overview of Ice Nucleating Particles, <https://doi.org/10.1175/AMSMONOGRAPH-D-16-0006.1>, 2017.

1080 Kärcher, B.: Cirrus Clouds and Their Response to Anthropogenic Activities, *Curr Clim Change Rep*, 3, 45–57, <https://doi.org/10.1007/s40641-017-0060-3>, 2017.

Kärcher, B., DeMott, P. J., Jensen, E. J., and Harrington, J. Y.: Studies on the Competition Between Homogeneous and Heterogeneous Ice Nucleation in Cirrus Formation, *Journal of Geophysical Research: Atmospheres*, 127, e2021JD035805, <https://doi.org/10.1029/2021JD035805>, 2022.

1085 Kärcher, B., Hoffmann, F., Sokol, A. B., Gasparini, B., Corcos, M., Jensen, E., Atlas, R., Podglajen, A., Morrison, H., Hertzog, A., Plougonven, R., Chandrasekhar, K. K., and Grabowski, W. W.: Dissecting cirrus clouds: navigating effects of turbulence on homogeneous ice formation, *npj Clim Atmos Sci*, 8, 137, <https://doi.org/10.1038/s41612-025-01024-w>, 2025.

1090 Kay, J. E., Hillman, B. R., Klein, S. A., Zhang, Y., Medeiros, B., Pincus, R., Gettelman, A., Eaton, B., Boyle, J., and Marchand, R.: Exposing global cloud biases in the Community Atmosphere Model (CAM) using satellite observations and their corresponding instrument simulators, *Journal of Climate*, 25, 5190–5207, <https://doi.org/10.1175/JCLI-D-11-00469.1>, 2012.

1095 Khvorostyanov, V. I. and Sassen, K.: Cirrus Cloud Simulation Using Explicit Microphysics and Radiation. Part I: Model Description, *Journal of the Atmospheric Sciences*, 55, 1808–1821, [https://doi.org/10.1175/1520-0469\(1998\)055<1808:CCSUEM>2.0.CO;2](https://doi.org/10.1175/1520-0469(1998)055<1808:CCSUEM>2.0.CO;2), 1998.

Krämer, M., Rolf, C., Luebke, A., Afchine, A., Spelten, N., Costa, A., Meyer, J., Zöger, M., Smith, J., Herman, R. L., Buchholz, B., Ebert, V., Baumgardner, D., Borrmann, S., Klingebiel, M., and Avallone, L.: A microphysics guide to cirrus clouds – Part 1: Cirrus types, *Atmos. Chem. Phys.*, 16, 3463–3483, <https://doi.org/10.5194/acp-16-3463-2016>, 2016.

Krämer, M., Rolf, C., Spelten, N., Afchine, A., Fahey, D., Jensen, E., Khaykin, S., Kuhn, T., Lawson, P., Lykov, A., Pan, L. L., Riese, M., Rollins, A., Stroh, F., Thornberry, T., Wolf, V.,

1100 Woods, S., Spichtinger, P., Quaas, J., and Sourdeval, O.: A microphysics guide to cirrus – Part 2: Climatologies of clouds and humidity from observations, *Atmospheric Chemistry and Physics*, 20, 12569–12608, <https://doi.org/10.5194/acp-20-12569-2020>, 2020.

1105 Kriegler, E., Luderer, G., Bauer, N., Baumstark, L., Fujimori, S., Popp, A., Rogelj, J., Strefler, J., and van Vuuren, D. P.: Pathways limiting warming to 1.5°C: a tale of turning around in no time?, *Philosophical Transactions of the Royal Society A: Mathematical, Physical and Engineering Sciences*, 376, 20160457, <https://doi.org/10.1098/rsta.2016.0457>, 2018.

1110 Lawson, R. P., Woods, S., Jensen, E., Erfani, E., Gurganus, C., Gallagher, M., Connolly, P., Whiteway, J., Baran, A. J., May, P., Heymsfield, A., Schmitt, C. G., McFarquhar, G., Um, J., Protat, A., Bailey, M., Lance, S., Muehlbauer, A., Stith, J., Korolev, A., Toon, O. B., and Krämer, M.: A Review of Ice Particle Shapes in Cirrus formed In Situ and in Anvils, *Journal of Geophysical Research: Atmospheres*, 124, 10049–10090, <https://doi.org/10.1029/2018JD030122>, 2019.

1115 Li, Q. and Groß, S.: Changes in cirrus cloud properties and occurrence over Europe during the COVID-19-caused air traffic reduction, *Atmos. Chem. Phys.*, 21, 14573–14590, <https://doi.org/10.5194/acp-21-14573-2021>, 2021.

1120 Lin, L., Liu, X., Zhao, X., Shan, Y., Ke, Z., Lyu, K., and Bowman, K. P.: Ice nucleation by volcanic ash greatly alters cirrus cloud properties, *Science Advances*, 11, eads0572, <https://doi.org/10.1126/sciadv.ads0572>, 2025.

Liu, Y. and Key, J. R.: Assessment of Arctic Cloud Cover Anomalies in Atmospheric Reanalysis Products Using Satellite Data, <https://doi.org/10.1175/JCLI-D-15-0861.1>, 2016.

1125 Loeb, N. G., Wielicki, B. A., Doelling, D. R., Smith, G. L., Keyes, D. F., Kato, S., Manalo-Smith, N., and Wong, T.: Toward Optimal Closure of the Earth’s Top-of-Atmosphere Radiation Budget, *Journal of Climate*, 22, 748–766, <https://doi.org/10.1175/2008JCLI2637.1>, 2009.

Lohmann, U. and Gasparini, B.: A cirrus cloud climate dial?, *Science*, 357, 248–249, <https://doi.org/10.1126/science.aan3325>, 2017.

1130 Lyu, K., Liu, X., Bacmeister, J., Zhao, X., Lin, L., Shi, Y., and Sourdeval, O.: Orographic Cirrus and Its Radiative Forcing in NCAR CAM6, *Journal of Geophysical Research: Atmospheres*, 128, e2022JD038164, <https://doi.org/10.1029/2022JD038164>, 2023.

Maciel, F. V., Diao, M., and Patnaude, R.: Examination of aerosol indirect effects during cirrus cloud evolution, *Atmospheric Chemistry and Physics*, 23, 1103–1129, <https://doi.org/10.5194/acp-23-1103-2023>, 2023.

Macke, A., Francis, P. N., McFarquhar, G. M., and Kinne, S.: The Role of Ice Particle Shapes and Size Distributions in the Single Scattering Properties of Cirrus Clouds, *Journal of the Atmospheric Sciences*, 55, 2874–2883, [https://doi.org/10.1175/1520-0469\(1998\)055<2874:TROIPS>2.0.CO;2](https://doi.org/10.1175/1520-0469(1998)055<2874:TROIPS>2.0.CO;2), 1998.

1135 Magurno, D., Cossich, W., Maestri, T., Bantges, R., Brindley, H., Fox, S., Harlow, C., Murray, J., Pickering, J., Warwick, L., and Oetjen, H.: Cirrus Cloud Identification from Airborne Far-Infrared and Mid-Infrared Spectra, *Remote Sensing*, 12, 2097, <https://doi.org/10.3390/rs12132097>, 2020.

1140 Maillard, J., Ravetta, F., Raut, J.-C., Mariage, V., and Pelon, J.: Characterisation and surface radiative impact of Arctic low clouds from the IAOOS field experiment, *Atmos. Chem. Phys.*, 21, 4079–4101, <https://doi.org/10.5194/acp-21-4079-2021>, 2021.

1145 Marsing, A., Meerkötter, R., Heller, R., Kaufmann, S., Jurkat-Witschas, T., Krämer, M., Rolf, C., and Voigt, C.: Investigating the radiative effect of Arctic cirrus measured in situ during the winter 2015–2016, *Atmospheric Chemistry and Physics*, 23, 587–609, <https://doi.org/10.5194/acp-23-587-2023>, 2023.

Matus, A. V. and L'Ecuyer, T. S.: The role of cloud phase in Earth's radiation budget: CLOUD PHASE IN EARTH'S RADIATION BUDGET, *J. Geophys. Res. Atmos.*, 122, 2559–2578, <https://doi.org/10.1002/2016JD025951>, 2017.

1150 Mitchell, D. L. and Erfani, E.: Cirrus Cloud Thinning, in: *Geoengineering and Climate Change*, John Wiley & Sons, Ltd, 297–306, <https://doi.org/10.1002/9781394204847.ch18>, 2025.

Mitchell, D. L. and Finnegan, W.: Modification of cirrus clouds to reduce global warming, *Environ. Res. Lett.*, 4, 045102, <https://doi.org/10.1088/1748-9326/4/4/045102>, 2009.

1155 Mitchell, D. L. and Garnier, A.: Advances in CALIPSO (IIR) cirrus cloud property retrievals. Part 2: Global estimates of the fraction of cirrus clouds affected by homogeneous ice nucleation, <https://doi.org/10.5194/egusphere-2024-3814>, 12 December 2024.

Mitchell, D. L., Garnier, A., Pelon, J., and Erfani, E.: CALIPSO (IIR–CALIOP) retrievals of cirrus cloud ice-particle concentrations, *Atmospheric Chemistry and Physics*, 18, 17325–17354, <https://doi.org/10.5194/acp-18-17325-2018>, 2018.

1160 Mitchell, D. L., Mejia, J., Garnier, A., Tomii, Y., Krämer, M., and Hosseinpour, F.: An Estimate of Global, Regional and Seasonal Cirrus Cloud Radiative Effects Contributed by Homogeneous Ice Nucleation, *Atmospheric Chemistry and Physics Discussions*, 1–48, <https://doi.org/10.5194/acp-2020-846>, 2020.

1165 Mitchell, D. L., Garnier, A. E., and Woods, S.: Advances in CALIPSO (IIR) cirrus cloud property retrievals – Part 1: Methods and testing, *EGUphere*, 1–44, <https://doi.org/10.5194/egusphere-2024-3790>, 2024.

Monroe, E. E., Taylor, P. C., and Boisvert, L. N.: Arctic Cloud Response to a Perturbation in Sea Ice Concentration: The North Water Polynya, *JGR Atmospheres*, 126, <https://doi.org/10.1029/2020JD034409>, 2021.

1170 Moschos, V., Dzepina, K., Bhattu, D., Lamkaddam, H., Casotto, R., Daellenbach, K. R., Canonaco, F., Rai, P., Aas, W., Becagli, S., Calzolai, G., Eleftheriadis, K., Moffett, C. E., Schnelle-Kreis, J., Severi, M., Sharma, S., Skov, H., Vestenius, M., Zhang, W., Hakola, H.,

1175 Hellén, H., Huang, L., Jaffrezo, J.-L., Massling, A., Nøjgaard, J. K., Petäjä, T., Popovicheva, O., Sheesley, R. J., Traversi, R., Yttri, K. E., Schmale, J., Prévôt, A. S. H., Baltensperger, U., and El Haddad, I.: Equal abundance of summertime natural and wintertime anthropogenic Arctic organic aerosols, *Nat. Geosci.*, 15, 196–202, <https://doi.org/10.1038/s41561-021-00891-1>, 2022.

NASEM report: Reflecting Sunlight: Recommendations for Solar Geoengineering Research and Research Governance, The national academies press, Washington, D.C., <https://doi.org/10.17226/25762>, 2021.

1180 Nazaryan, H., McCormick, M. P., and Menzel, W. P.: Global characterization of cirrus clouds using CALIPSO data, *J. Geophys. Res.*, 113, D16211, <https://doi.org/10.1029/2007JD009481>, 2008.

Ngo, D., Diao, M., Patnaude, R. J., Woods, S., and Diskin, G.: Aerosol Indirect Effects on Cirrus Clouds Based on Global-Scale Airborne Observations and Machine Learning Models, *EGUphere*, 1–36, <https://doi.org/10.5194/eguph-2024-2122>, 2024.

1185 Patnaude, R. and Diao, M.: Aerosol Indirect Effects on Cirrus Clouds Based on Global Aircraft Observations, *Geophysical Research Letters*, 47, e2019GL086550, <https://doi.org/10.1029/2019GL086550>, 2020.

1190 Patnaude, R., Diao, M., Liu, X., and Chu, S.: Effects of thermodynamics, dynamics and aerosols on cirrus clouds based on in situ observations and NCAR CAM6, *Atmospheric Chemistry and Physics*, 21, 1835–1859, <https://doi.org/10.5194/acp-21-1835-2021>, 2021.

Penner, J. E., Zhou, C., and Liu, X.: Can cirrus cloud seeding be used for geoengineering?, *Geophysical Research Letters*, 42, 8775–8782, <https://doi.org/10.1002/2015GL065992>, 2015.

1195 Pereira, L., Morrow, D., Aquila, V., Beckage, B., Beckbesinger, S., Beukes, L., Buck, H., Carlson, C., Geden, O., Jones, A., Keller, D., Mach, K., Mashigo, M., Moreno-Cruz, J., Visioni, D., Nicholson, S., and Trisos, C.: From fAIrplay to climate wars: making climate change scenarios more dynamic, creative, and integrative, *Ecology and Society*, 26, <https://doi.org/10.5751/ES-12856-260430>, 2021.

1200 Philipp, D., Stengel, M., and Ahrens, B.: Analyzing the Arctic Feedback Mechanism between Sea Ice and Low-Level Clouds Using 34 Years of Satellite Observations, *Journal of Climate*, 33, 7479–7501, <https://doi.org/10.1175/JCLI-D-19-0895.1>, 2020.

Rantanen, M., Karpechko, A. Y., Lipponen, A., Nordling, K., Hyvärinen, O., Ruosteenoja, K., Vihma, T., and Laaksonen, A.: The Arctic has warmed nearly four times faster than the globe since 1979, *Commun Earth Environ*, 3, 1–10, <https://doi.org/10.1038/s43247-022-00498-3>, 2022.

1205 Roskovensky, J. K. and Liou, K. N.: Detection of thin cirrus from 1.38  $\mu\text{m}$ /0.65  $\mu\text{m}$  reflectance ratio combined with 8.6–11  $\mu\text{m}$  brightness temperature difference, *Geophysical Research Letters*, 30, <https://doi.org/10.1029/2003GL018135>, 2003.

Samset, B. H., Stjern, C. W., Andrews, E., Kahn, R. A., Myhre, G., Schulz, M., and Schuster, G. L.: Aerosol Absorption: Progress Towards Global and Regional Constraints, *Curr Clim Change Rep.*, 4, 65–83, <https://doi.org/10.1007/s40641-018-0091-4>, 2018.

1210 Sassen, K., Wang, Z., and Liu, D.: Cirrus clouds and deep convection in the tropics: Insights from CALIPSO and CloudSat, *J. Geophys. Res.*, 114, D00H06, <https://doi.org/10.1029/2009JD011916>, 2009.

Schläpfer, D., Richter, R., and Reinartz, P.: Elevation-Dependent Removal of Cirrus Clouds in Satellite Imagery, *Remote Sensing*, 12, 494, <https://doi.org/10.3390/rs12030494>, 2020.

1215 Schmale, J., Sharma, S., Decesari, S., Pernov, J., Massling, A., Hansson, H.-C., von Salzen, K., Skov, H., Andrews, E., Quinn, P. K., Upchurch, L. M., Eleftheriadis, K., Traversi, R., Gilardoni, S., Mazzola, M., Laing, J., and Hopke, P.: Pan-Arctic seasonal cycles and long-term trends of aerosol properties from 10 observatories, *Atmos. Chem. Phys.*, 22, 3067–3096, <https://doi.org/10.5194/acp-22-3067-2022>, 2022.

1220 Schumann, U., Mayer, B., Graf, K., and Mannstein, H.: A Parametric Radiative Forcing Model for Contrail Cirrus, *Journal of Applied Meteorology and Climatology*, 51, 1391–1406, <https://doi.org/10.1175/JAMC-D-11-0242.1>, 2012.

Schweiger, A. J.: Changes in seasonal cloud cover over the Arctic seas from satellite and surface observations, *Geophysical Research Letters*, 31, <https://doi.org/10.1029/2004GL020067>, 2004.

1225 Screen, J. A. and Simmonds, I.: The central role of diminishing sea ice in recent Arctic temperature amplification, *Nature*, 464, 1334–1337, <https://doi.org/10.1038/nature09051>, 2010.

Shettle, E. P.: Models of aerosols, clouds, and precipitation for atmospheric propagation studies, in: In AGARD Conference Proceedings, ADS Bibcode: 1990apuv.agar.....S, 1989.

1230 Shi, X., Liu, X., and Zhang, K.: Effects of pre-existing ice crystals on cirrus clouds and comparison between different ice nucleation parameterizations with the Community Atmosphere Model (CAM5), *Atmospheric Chemistry and Physics*, 15, 1503–1520, <https://doi.org/10.5194/acp-15-1503-2015>, 2015.

1235 Sourdeval, O., Gryspierdt, E., Krämer, M., Goren, T., Delanoë, J., Afchine, A., Hemmer, F., and Quaas, J.: Ice crystal number concentration estimates from lidar–radar satellite remote sensing – Part 1: Method and evaluation, *Atmospheric Chemistry and Physics*, 18, 14327–14350, <https://doi.org/10.5194/acp-18-14327-2018>, 2018.

Spichtinger, P. and Cziczo, D. J.: Impact of heterogeneous ice nuclei on homogeneous freezing events in cirrus clouds, *Journal of Geophysical Research: Atmospheres*, 115, <https://doi.org/10.1029/2009JD012168>, 2010.

1240 Spichtinger, P. and Gierens, K. M.: Modelling of cirrus clouds – Part 2: Competition of different nucleation mechanisms, *Atmospheric Chemistry and Physics*, 9, 2319–2334, <https://doi.org/10.5194/acp-9-2319-2009>, 2009.

1245 Sporre, M. K., Friberg, J., Svenhag, C., Sourdeval, O., and Storelvmo, T.: Springtime  
Stratospheric Volcanic Aerosol Impact on Midlatitude Cirrus Clouds, *Geophysical Research Letters*, 49, <https://doi.org/10.1029/2021GL096171>, 2022.

Stamnes, K., Tsay, S.-C., Wiscombe, W., and Laszlo, I.: DISORT, a general-purpose Fortran  
program for discrete-ordinate-method radiative transfer in scattering and emitting layered media:  
documentation of methodology, 2000.

1250 Steffen, W., Rockström, J., Richardson, K., Lenton, T. M., Folke, C., Liverman, D.,  
Summerhayes, C. P., Barnosky, A. D., Cornell, S. E., Crucifix, M., Donges, J. F., Fetzer, I.,  
Lade, S. J., Scheffer, M., Winkelmann, R., and Schellnhuber, H. J.: Trajectories of the Earth  
System in the Anthropocene, *Proceedings of the National Academy of Sciences*, 115, 8252–  
8259, <https://doi.org/10.1073/pnas.1810141115>, 2018.

1255 Stephens, G. L., Tsay, S.-C., Stackhouse, P. W., and Flatau, P. J.: The Relevance of the  
Microphysical and Radiative Properties of Cirrus Clouds to Climate and Climatic Feedback,  
1990.

Storelvmo, T. and Herger, N.: Cirrus cloud susceptibility to the injection of ice nuclei in the  
upper troposphere, *Journal of Geophysical Research: Atmospheres*, 119, 2375–2389,  
<https://doi.org/10.1002/2013JD020816>, 2014.

1260 Storelvmo, T., Kristjansson, J. E., Muri, H., Pfeffer, M., Barahona, D., and Nenes, A.: Cirrus  
cloud seeding has potential to cool climate, *Geophysical Research Letters*, 40, 178–182,  
<https://doi.org/10.1029/2012GL054201>, 2013.

1265 Storelvmo, T., Boos, W. R., and Herger, N.: Cirrus cloud seeding: a climate engineering  
mechanism with reduced side effects?, *Philosophical Transactions of the Royal Society A:  
Mathematical, Physical and Engineering Sciences*, 372, 20140116,  
<https://doi.org/10.1098/rsta.2014.0116>, 2014.

Stubenrauch, C. J., Chédin, A., Rädel, G., Scott, N. A., and Serrar, S.: Cloud Properties and  
Their Seasonal and Diurnal Variability from TOVS Path-B, *Journal of Climate*, 19, 5531–5553,  
<https://doi.org/10.1175/JCLI3929.1>, 2006.

1270 Stubenrauch, C. J., Cros, S., Lamquin, N., Armante, R., Chédin, A., Crevoisier, C., and Scott, N.  
A.: Cloud properties from Atmospheric Infrared Sounder and evaluation with Cloud-Aerosol  
Lidar and Infrared Pathfinder Satellite Observations, *J. Geophys. Res.*, 113, D00A10,  
<https://doi.org/10.1029/2008JD009928>, 2008.

1275 Sun, W., Videen, G., Kato, S., Lin, B., Lukashin, C., and Hu, Y.: A study of subvisual clouds  
and their radiation effect with a synergy of CERES, MODIS, CALIPSO, and AIRS data, *Journal  
of Geophysical Research: Atmospheres*, 116, <https://doi.org/10.1029/2011JD016422>, 2011.

Takano, Y., Liou, K. N., and Minnis, P.: The Effects of Small Ice Crystals on Cirrus Infrared  
Radiative Properties, *Journal of the Atmospheric Sciences*, 49, 1487–1493,  
[https://doi.org/10.1175/1520-0469\(1992\)049<1487:TEOSIC>2.0.CO;2](https://doi.org/10.1175/1520-0469(1992)049<1487:TEOSIC>2.0.CO;2), 1992.

1280 Tan, X., Huang, Y., Diao, M., Bansemer, A., Zondlo, M. A., DiGangi, J. P., Volkamer, R., and Hu, Y.: An assessment of the radiative effects of ice supersaturation based on in situ observations, *Geophysical Research Letters*, 43, 11,039-11,047, <https://doi.org/10.1002/2016GL071144>, 2016.

1285 Tierney, J. E., King, J., Osman, M. B., Abell, J. T., Burls, N. J., Erfani, E., Cooper, V. T., and Feng, R.: Pliocene Warmth and Patterns of Climate Change Inferred From Paleoclimate Data Assimilation, *AGU Advances*, 6, e2024AV001356, <https://doi.org/10.1029/2024AV001356>, 2025.

1290 Tully, C., Neubauer, D., Omanovic, N., and Lohmann, U.: Cirrus cloud thinning using a more physically based ice microphysics scheme in the ECHAM-HAM general circulation model, *Atmos. Chem. Phys.*, 22, 11455–11484, <https://doi.org/10.5194/acp-22-11455-2022>, 2022.

Tully, C., Neubauer, D., Villanueva, D., and Lohmann, U.: Does prognostic seeding along flight tracks produce the desired effects of cirrus cloud thinning?, *Atmospheric Chemistry and Physics*, 23, 7673–7698, <https://doi.org/10.5194/acp-23-7673-2023>, 2023.

1295 Villanueva, D., Possner, A., Neubauer, D., Gasparini, B., Lohmann, U., and Tesche, M.: Mixed-phase regime cloud thinning could help restore sea ice, *Environ. Res. Lett.*, 17, 114057, <https://doi.org/10.1088/1748-9326/aca16d>, 2022.

1300 Wang, J., Liu, C., Yao, B., Min, M., Letu, H., Yin, Y., and Yung, Y. L.: A multilayer cloud detection algorithm for the Suomi-NPP Visible Infrared Imager Radiometer Suite (VIIRS), *Remote Sensing of Environment*, 227, 1–11, <https://doi.org/10.1016/j.rse.2019.02.024>, 2019.

1305 Wang, J. R., Liu, G., Spinhirne, J. D., Racette, P., and Hart, W. D.: Observations and retrievals of cirrus cloud parameters using multichannel millimeter-wave radiometric measurements, *J. Geophys. Res.*, 106, 15251–15263, <https://doi.org/10.1029/2000JD900262>, 2001.

Wang, X. and Key, J. R.: Recent Trends in Arctic Surface, Cloud, and Radiation Properties from Space, *Science*, 299, 1725–1728, <https://doi.org/10.1126/science.1078065>, 2003.

1310 Wilber, A. C., Kratz, D. P., and Gupta, S. K.: Surface Emissivity Maps for Use in Satellite Retrievals of Longwave Radiation, *NASA Scientific and Technical Information*, 1999.

Wolf, K., Bellouin, N., and Boucher, O.: Radiative effect by cirrus cloud and contrails – A comprehensive sensitivity study, *Radiation/Atmospheric Modelling/Troposphere/Physics (physical properties and processes)*, <https://doi.org/10.5194/egusphere-2023-155>, 2023.

1315 Wu, D. L., Lambert, A., Read, W. G., Eriksson, P., and Gong, J.: MLS and CALIOP Cloud Ice Measurements in the Upper Troposphere: A Constraint from Microwave on Cloud Microphysics, *Journal of Applied Meteorology and Climatology*, 53, 157–165, <https://doi.org/10.1175/JAMC-D-13-041.1>, 2014.

Xie, H., Wang, Z., Luo, T., Yang, K., Zhang, D., Zhou, T., Yang, X., Liu, X., and Fu, Q.: Seasonal Variation of Dust Aerosol Vertical Distribution in Arctic Based on Polarized

Micropulse Lidar Measurement, *Remote Sensing*, 14, 5581, <https://doi.org/10.3390/rs14215581>, 2022.

1320 Yorks, J. E., Wang, J., McGill, M. J., Follette-Cook, M., Nowotnick, E. P., Reid, J. S., Colarco, P. R., Zhang, J., Kalashnikova, O., Yu, H., Marenco, F., Santanello, J. A., Weckwerth, T. M., Li, Z., Campbell, J. R., Yang, P., Diao, M., Noel, V., Meyer, K. G., Carr, J. L., Garay, M., Christian, K., Bennedetti, A., Ring, A. M., Crawford, A., Pavolonis, M. J., Aquila, V., Kim, J., and Kondragunta, S.: A SmallSat Concept to Resolve Diurnal and Vertical Variations of Aerosols, Clouds, and Boundary Layer Height, *Bulletin of the American Meteorological Society*, <https://doi.org/10.1175/BAMS-D-21-0179.1>, 2023.

1325 Yu, Y., Taylor, P. C., and Cai, M.: Seasonal Variations of Arctic Low-Level Clouds and Its Linkage to Sea Ice Seasonal Variations, *Journal of Geophysical Research: Atmospheres*, 124, 12206–12226, <https://doi.org/10.1029/2019JD031014>, 2019.

1330 Yue, Q., Jiang, J. H., Heymsfield, A., Liou, K., Gu, Y., and Sinha, A.: Combining In Situ and Satellite Observations to Understand the Vertical Structure of Tropical Anvil Cloud Microphysical Properties During the TC4 Experiment, *Earth and Space Science*, 7, <https://doi.org/10.1029/2020EA001147>, 2020.

1335 Zamora, L. M., Kahn, R. A., Cubison, M. J., Diskin, G. S., Jimenez, J. L., Kondo, Y., McFarquhar, G. M., Nenes, A., Thornhill, K. L., Wisthaler, A., Zelenyuk, A., and Ziemba, L. D.: Aircraft-measured indirect cloud effects from biomass burning smoke in the Arctic and subarctic, *Atmospheric Chemistry and Physics*, 16, 715–738, <https://doi.org/10.5194/acp-16-715-2016>, 2016.

1340 Zhang, Y., Macke, A., and Albers, F.: Effect of crystal size spectrum and crystal shape on stratiform cirrus radiative forcing, *Atmospheric Research*, 52, 59–75, [https://doi.org/10.1016/S0169-8095\(99\)00026-5](https://doi.org/10.1016/S0169-8095(99)00026-5), 1999.

1345 Zhou, Y., Sun, X., Zhang, R., Zhang, C., Li, H., Zhou, J., and Li, S.: Influences of cloud heterogeneity on cirrus optical properties retrieved from the visible and near-infrared channels of MODIS/SEVIRI for flat and optically thick cirrus clouds, *Journal of Quantitative Spectroscopy and Radiative Transfer*, 187, 232–246, <https://doi.org/10.1016/j.jqsrt.2016.09.020>, 2017.

Zhu, X., Wang, Z., Liu, D., and Cai, H.: The First Global Insight of Cirrus Clouds Characterized by Hollow Ice Crystals From Space-Borne Lidar, *Geophysical Research Letters*, 51, e2024GL109852, <https://doi.org/10.1029/2024GL109852>, 2024.